Investigating the Operating Mechanism of a Diffraction Based BioSensor

A Thesis Submitted to the

College of Graduate Studies and Research

in Partial Fulfillment of the Requirements

for the degree of Master of Science

in the Department of Chemistry

University of Saskatchewan

Saskatoon

By

Jahangir Jafferali Valiani

PERMISSION TO USE

In presenting this thesis in partial fulfilment of the requirements for a Postgraduate degree from the University of Saskatchewan, I agree that the Libraries of this University may make it freely available for inspection. I further agree that permission for copying of this thesis in any manner, in whole or in part, for scholarly purposes may be granted by the professor or professors who supervised my thesis work or, in their absence, by the Head of the Department or the Dean of the College in which my thesis work was done. It is understood that any copying or publication or use of this thesis or parts thereof for financial gain shall not be allowed without my written permission. It is also understood that due recognition shall be given to me and to the University of Saskatchewan in any scholarly use which may be made of any material in my thesis.

Requests for permission to copy or to make other use of material in this thesis in whole or part should be addressed to:

> Head of the Department of Chemistry
>
> 163 Thorvaldson Building
>
> 110 Science Place
>
> University of Saskatchewan
>
> Saskatoon, Saskatchewan
>
> Canada
>
> S7N 5C9

ABSTRACT

In this work, we describe our recent efforts aimed at determining the mechanism of signal change for a diffraction-based sensor (DBS) system. The DBS detects analyte-binding events by monitoring the change in diffraction efficiency that takes place when analyte molecules adsorb to target molecules that have been patterned onto a surface. The exact parameters that affect the intensity of the diffraction intensity are currently not well understood.

In this work, the formalism used to describe the behaviour of volume-phase holography is used to understand the parameters that effect the diffraction intensity. It is hypothesized that the major factors that effect the diffraction intensity are the differences in optical path length between the wave trains that reflect off the diffraction grating and those that reflect off the substrate surface. Also key is the difference in refractive index between the two media. Two approaches were developed to investigate this hypothesis; the first was to develop a series of gratings of varying thickness using polyelectrolyte multilayers. The indices of refraction of these gratings were adjusted by the incorporation of charged gold nanoparticles. Since DBS systems operate by monitoring the binding of analyte molecules, a second series of experiments were developed to investigate the changes in diffraction intensity as 2 μm carboxylated beads were loaded onto an avidin grating. The first aspect that was investigated was the effect of adding more particles onto the grating surface on diffraction intensity. Second, the extent to which the particles reduced the periodicity of the diffraction grating, and the effect on the observed intensity of the diffraction signal were also investigated. Finally, this work shows the first use of a DBS system to extract the rate of and the maximum surface coverage of a specific binding reaction.

Acknowledgements

scheduling everything, and significantly reducing the amount of paper work that I had to complete.

Noting that people who read this will pay particular attention to those at the beginning and at the end, I would like to conclude by extending my deepest gratitude to my family. With out their love and support I would not have been able to accomplish even a portion of the tasks required to complete this degree. This includes, but is not limited to, my parents, Jafferali and Gulshan Valiani, my sister and brother-in-law, Waqar-un-nissa and Daniel T. Ressl, my niece and nephew, Matina and Danial Ressl, and finally my cousins, Rahim, Nadim, Pervez, Rahil, and Salimah Valiani and Nadeem Bhatia.

This work is dedicated to Shirin J. Valiani. In loving memory.

CONTENTS

LIST OF TABLES

List of Figures

LIST OF ABBREVIATIONS

AFM — Atomic Force Microscopy
DBS — Diffraction Based Sensor
DMAP — 4-dimethyl aminopyridine
η — Diffraction Efficiency
LBL — Layer-by-layer deposition technique
PAH — Poly(allyl amine hydrochloride)
PBD — Polybutadiene
PDAC — Poly(diallyl dimethylammonium chloride)
PDMS — Poly(dimethyl siloxane)
PE — Polyelectrolyte
PECH — Polyepichlorohydrin
PIB — Polyisobutylene
PS — Polystyrene
PSS — Poly(styrene sulfonic acid) sodium salt
TALH — Titanium(IV) bis(ammonium lactato)dihidroxide
TEM — Transmission electron microscopy
TOAB — Tetraoctylammonium bromide
VPH — Volume-phase holography

CHAPTER 1

INTRODUCTION

1.1 Background of diffraction based sensing

1.1.1 Motivation for developing diffraction based sensors

Detection and quantification of analytes is the central focus of analytical chemistry. A wide variety of analytical methods have been developed to accurately detect and quantify molecules of interest. Of particular interest in bioanalytical chemistry is the detection of biological molecules. A common approach to detecting and quantifying biomolecules are immunoassays. Immunoassays are tests that use the binding of antigens to their complementary antibodies. Detection of this binding, however, usually requires a large number of processing steps to make the analyte detectable[1]. An analytical method for detecting biomolecules that requires minimal sample preparation and can be used for a wide range of analytes is highly desirable. Diffraction based sensing has the potential to detect and quantify many different kinds of analytes with minimal processing of the analyte.

In recent years chemical sensors based on the principles of optical diffraction have gained attention because of the speed, selectivity, and versatility of these methods [2, 3, 4]. These diffraction based sensors (DBSs) require a "target" molecule to be patterned in a periodic array onto a substrate surface. When the target is illuminated with light, the target molecules create a diffraction pattern. A solution containing an analyte molecule that will bind to the "target" molecules is then passed over the substrate. Binding of the analyte to the target molecules results in an increase in the intensity of the diffraction spots. This simple mechanism allows the instrument

1

to sense a variety of different analytes without major modification to the sensing apparatus.

The advantages of the DBS become obvious when compared to immunoassays. The most ubiquitous immunoassays involve labeling the desired analyte with a fluorophore or other label. The extra processing of the target molecule makes such tests time consuming and labour intensive. Immunoassays that do not require processing of the target molecule typically cannot reach detection limits required, and are often cost prohibitive. The DBS system does not require this extra sample processing.

1.1.2   Early developments in diffraction-based sensing

One of the greatest strengths of DBSs is their ability to be applied to a variety of analytes. Almost any analyte can be detected as long as its target molecule can be printed onto a substrate. The number of materials that the diffraction grating can be made from is almost limitless. This gives this class of chemical sensors a wide range of possible targets with no modification of the main apparatus needed. By merely printing different types of biomolecules, one can analyze proteins[1, 2, 3, 4, 6, 5, 7], cells[7], and DNA[8]. This approach has even been extended to analyze certain classes of inorganic compounds[9, 10, 11].

Diffraction based sensing was originally developed as an inexpensive, user friendly method to perform immunoassays[1]. In this original system, an antibody or antigen is coated onto a silicon surface. A photomask with the diffraction grating pattern, is placed over the coated wafer and the exposed areas are inactivated by UV illumination. Binding of the analyte molecule, therefore, can only occur on the periodically active areas of the surface. This binding will then cause the appearance of a diffraction pattern.

Diffraction based sensing as a diagnostic tool and one that could be used in quantification of interactions of bio-molecular systems was brought to the forefront by the Goh[2, 3, 4, 5] and Paige[6] groups. These groups have investigated the use of the DBS for detection and quantification of a number of important analytes. Of particular note was the ability for a DBS to simultaneously monitor the binding of multiple

analytes as a function of time (Goh et al.[5]). Since the observed diffraction pattern is a function of the orientation and spacing of the diffraction grating, it is possible to detect multiple analytes as long as their targets are patterned differently. This group has also attempted to significantly improve the detection limits of diffraction based sensing. Initial experiments on the original system developed by Tsay gave detection limits on the order of μg/mL[1]. Labeling the analyte with gold gave a 40-fold increase in detection limits (~ 25 ng/mL)[3]. More recently, detection limits on the order of pg/mL were achieved using secondary enzymatic amplification with a precipitating substrate[4].

The Paige group has demonstrated the use of DBSs to track simple enzyme kinetics in the IgG - trypsin system[6]. A grating made from mouse IgG was exposed to a solution of the enzyme trypsin. Diffraction intensity was monitored as a function of time and decayed exponentially. The Goh group[5] performed realtime monitoring of the mouse and rabbit IgG/anti-IgG system. Again, the diffraction intensity was reported as a function of time. Both these groups introduce the potential of diffraction based sensing as a tool to probe the kinetics of biological systems. However, without a deeper understanding of the quantitative factors that effect the diffraction intensity, the results give no further insight into what may be occurring at the molecular level.

Work outside the area of immunoassays and enzyme activity was performed by Nakajima[11]. A DBS system was made into a simple pH sensor by fabricating a grating from thymolphthalein and a 7% gelatin solution. The diffraction grating was then dipped into the solution to be analyzed. A solution with pH greater than 10.5 caused the grating with indicator to turn blue, and a diffraction pattern appeared when placed in the path of laser light. Below pH 10.5, the indicator would be transparent, and no diffraction pattern was observed. The pH range could be easily tuned by use of different indicators.

In another application, diffraction gratings made of several types of polymers were synthesized to detect the presence and quantity of a volatile organic compound[12]. Polymers, in general, are useful for the creation of diffraction gratings due to their

ability to act as receptors to a moderately wide set of target molecules. Three different polymers, Polyepichlorohydrin (PECH), Polyisobutylene (PIB), and Polybutadiene (PBD), were patterned onto a glass substrate using a diffraction template created from an atomic force microscopy (AFM) calibration grid. Known amounts of toluene, methyl ethyl ketone, hexane, and chloroform vapours were measured using a variety of gratings. Depending on the polymer that makes up the grating, the responses to various compounds varied largely. This work shows that, in principle it should be possible to create a grating that can identify a large number of volatile organic compounds. With a little data analysis, this data can then be used to identify an unknown or, perhaps, determine the concentration of a given analyte.

While a great deal of research has been devoted to the applications of DBS technology, little has been done to understand the underlying physics of how the diffraction based sensor operates. This work will focus on developing an understanding of how experimental parameters affect the measured diffraction signal in a quantitative way. The major parameters of interest are refractive index of the gratings, optical path length, and the extent of ordering of particles on the surface. This should also give greater insight into the results of experiments previously reported in the literature[3, 6] , especially when kinetic data are presented.

1.1.3 Nature of diffraction and diffraction efficiency

In its broadest sense, diffraction is the deviation of wavefronts from a parallel propagation. This is typically caused by an obstruction in the path of the wavefronts. When the wavefronts intersect they may constructively or destructively interfere with one another. The resulting pattern is called a diffraction pattern.

Two types of diffraction gratings are used in this research. The first are fabricated from polyelectrolytes on a glass substrate, while the second are made of avidin on a polystyrene (PS) substrate. We propose that diffraction in these systems is caused by the wave trains entering an area of periodic refractive index differences. The wave trains that enter the areas of higher refractive index will travel at a lower velocity. Once all the wave trains enter an area of common refractive index, they will be out

of phase with one another [13]. The interference that is caused by this will result in the observed diffraction pattern. Figure 1.1 shows this phenomenon.This is similar to the description used in the field of Volume-phase holography (VPH).
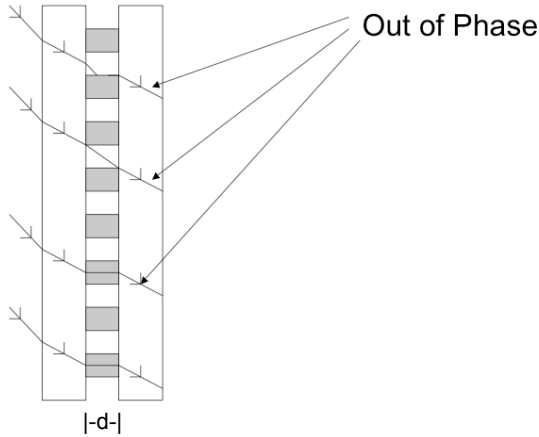
Figure 1.1: Schematic of diffraction occurring as light passes through region of periodic refractive index.

From VPH theory, diffraction efficiency, η, is described as the ratio of the intensity of the diffraction spot being observed, I_n, to the intensity of incoming beam of light, I_0(equation 1.1)[14].

$$\eta = \frac{I_n}{I_0} \tag{1.1}$$

The diffraction efficiency is controlled by both the optical path length, d, the modulation in refractive index, Δn, and the angle of incidence, α [15, 16, 17, 18]. As long as the optical path length of the grating multiplied by the wavelength of light, λ, is approximately 1.7 times larger than the product of the average refractive index and the square of the period of the grating, equation 1.2 adequately describes the diffraction efficiency of the grating.

$$\eta = \sin^2 \frac{\pi \Delta n d}{\lambda \cos \alpha} \tag{1.2}$$

This relationship is useful as it can be used to describe the observed intensity of a

diffraction signal as a function of the thickness and the modulation of the refractive index of the grating. If our proposal is correct, then the behaviour of the DBS system should follow that predicted by VPH theory.

1.1.4   Particle loading

As noted previously, DBSs operate by monitoring the change of intensity of diffraction as analyte molecules bind to the target. If the particles are large enough, we expect them to act in a manner similar to a thicker grating. In effect, we propose that loading of particles should act to change the optical path length of the system. This is exactly the same phenomenon that occurs by varying the grating thickness. We expect, therefore, that as more particles are loaded onto the surface, the intensity of the diffraction signal to increase in a similar manner as if the average grating thickness were being increased. Another factor that we believe may be important is to quantify the degree of order that the analyte molecules possess when adsorbed to the target grating. As particles were less ordered on the surface, we would expect the scattering between particles to play a more pronounced role to reduce the intensity of the observed diffraction signal via interference.

1.2   General experimental methodology

To determine how well the observed diffraction intensities follow the relationships developed for VPH gratings, a series of diffraction gratings were fabricated by printing patterned polyelectrolyte multilayers. The goal was to systematically vary the thickness of the grating (d) and the refractive index difference (Δn) In accordance with equation 1.2. In this section, background material on the printing process and on polyelectrolytes is provided. A somewhat different approach was taken for measuring the effect of particle loading, and this is described in more detail in Chapter 3.

1.2.1 Microcontact Printing

Microcontact printing is a nano-lithographic technique. It has been shown to effectively develop complex patterns of proteins and other molecules on a variety of surfaces[19]. We intend to use microcontact printing to develop diffraction gratings of polyelectrolyte multilayers onto a glass surface.

A patterned stamp is usually made by curing poly(dimethyl siloxane)(PDMS) on a template, which in this case is an acrylic diffraction grating. The patterned stamp is then inked in a solution of the molecules that are to be printed. Depending on the nature of the molecules and substrate (hydrophobic or hydrophilic, for example), the stamp may need to be treated to ensure that the molecules will preferentially bind to the substrate. The actual printing process involves pressing the stamp onto the substrate. In a protein system this printing technique has been shown to have better than 99% transfer efficiency after seconds of contact[19]. Again, the technique can be applied to a wide variety of systems by controlling the properties of the stamp and substrate to ensure that the molecules that form the pattern have a greater affinity for the substrate when compared to the stamp. Figure 1.2 shows a schematic of the microcontact printing technique.

1.2.2 Properties of polyelectrolyte multilayers

Self-assembled multilayers of polymers that possess multiple charges (herein referred to as polyelectrolytes) allow for the development of thin films with well defined thickness[20]. Polyelectrolytes are long chain polymers that exhibit extraordinarily high charge density. It is easy to take advantage of these high charge densities to form self-assembled films with a high degree of control over thickness[20, 21]. Generally, a charged solid substrate is placed in a solution of polyelectrolyte with the opposite charge. The strong multiple electrostatic interactions cause the polyelectrolyte to form a thin layer on the surface. This new layer will cause the exposed surface to have a charge opposite to the charge initially on the substrate. After rinsing, this sample is placed into a solution of an oppositely charged polyelectrolyte, which will
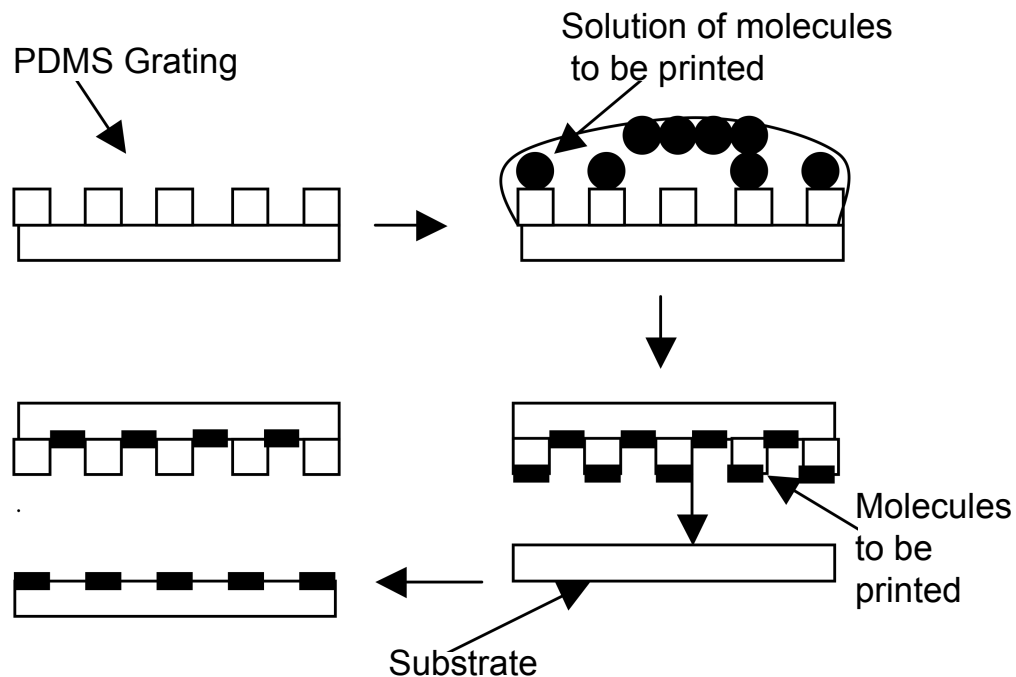
Figure 1.2: Schematic illustration of the microcontact printing procedure.

form a second layer on the surface causing the surface charge to revert to its original sign. This process is repeated until the desired thickness is achieved (Figure 1.3). Aside from varying the number of layers, it is possible to control the thickness of the multilayer films by varying the concentration of salt in the polyelectrolyte solutions. Since the salt causes the polyelectrolytes to fold in on themselves, surface roughness will also increase with increasing salt concentration[22].

These films are extremely stable because of the large number of charge neutralization interactions[23]. It has also been shown that any defects in the film structure tend to be hidden by the application of additional layers[20, 21]. This is due to the amorphous nature of these films[24]. Unlike the highly ordered Langmuir-Blodgett
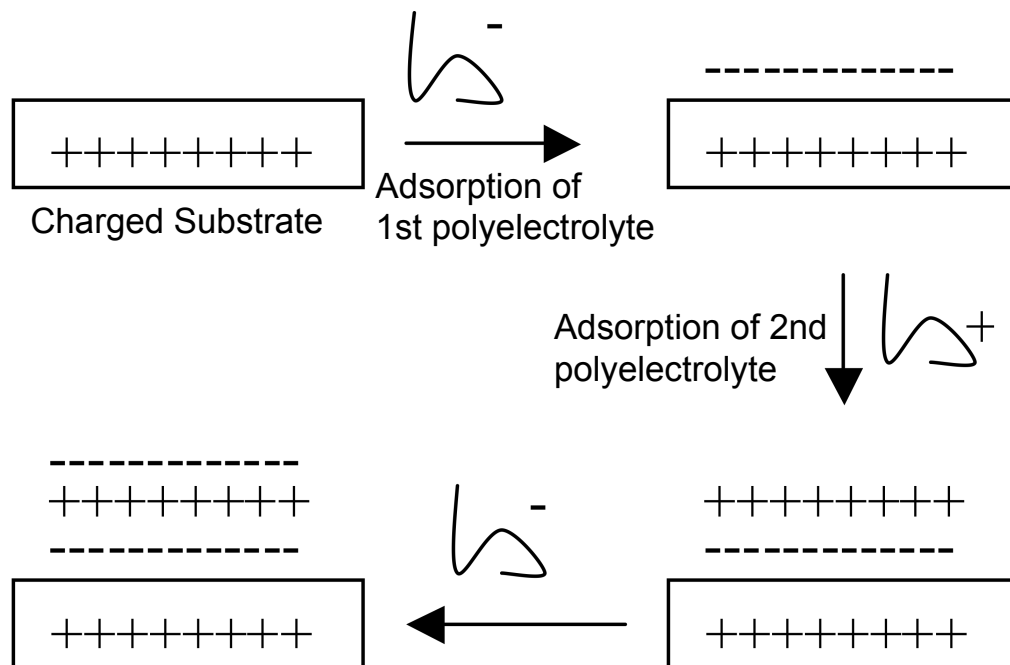
Figure 1.3: A simplified depiction of the layer by layer (LBL) deposition technique for polyelectrolytes.

films, the polyelectrolytes tend to interpenetrate with previously deposited layers.

Recently, multilayer films of polyelectrolytes have been patterned using a multilayer microcontact printing technique[25]. As in "normal" microcontact printing, the polyelectrolyte layers are deposited onto a PDMS stamp. The multilayers are transferred to the substrate because of more favorable interactions between the exposed layer and the substrate compared to that of the stamp and the polyelectrolyte adjacent to it.

Fabricating diffraction gratings out of polyelectrolyte multilayers will allow the relationship between the thickness and observed diffraction intensity to be elucidated in a systematic manner. In addition, the high charge density and semi-porosity

of polyelectrolytes allows for easy uptake of charged metal nanoparticles into the multilayers[26, 27, 28]. Uptake of nanoparticles can be used to change the refractive index of the multilayers and can be controlled by controlling the extent of loading of the nanoparticles.

1.3 Objectives

In this thesis, two approaches have been taken to gain a better understanding of and to quantify the factors that affect the intensity of the diffraction signal (diffraction efficiency). These two approaches investigated the effects of the grating properties, and the effects of analyte loading on signal intensity. The grating properties that are of primary interest are the effects of thickness and refractive index. This is accomplished by developing a series of gratings from polyelectrolyte multilayers. The thickness of the polyelectrolyte gratings was controlled by manipulating the number of layers of polyelectrolyte used and the salt concentration of the polyelectrolyte solutions. The refractive index of these gratings was manipulated by incorporating gold nanoparticles into the gratings. The effects of analyte loading and ordering were investigated at the lab of M. Cynthia Goh at the University of Toronto. Using the Axela dotLab^{TM} system, a solution of 2 μm PS beads with carboxyl groups on the surface was flowed over an avidin grating varying the time of exposure of the beads to the grating. The resulting diffraction intensity as a function of time data were interpreted to give kinetic parameters of the system. Optical microscopy of the sensor surface was then used to elucidate the effect of loading large particles onto the grating surface, and to begin to develop a method to quantify the effects of particle order on the signal.

CHAPTER 2

CHARACTERIZING THE EFFECT OF GRATING PROPERTIES ON DIFFRACTION EFFICIENCY

2.1 Materials and Methods

2.1.1 Preparation of polyelectrolyte multilayer gratings

PDMS stamps were made by curing the elastomeric polymer Sylgard 184 (Dow Corning) for eight hours on acrylic masters after leaving the sample for 1 hour to out-gas. The newly developed stamps were tested to confirm the transfer of the diffraction grating. This was accomplished by placing the stamp in the beam of a laser to observe if a diffraction pattern is produced. A sample of the template diffraction pattern is given in figure 2.1.

Patterned polyelectrolyte multilayers were printed on glass using microcontact printing. Stamps with the desired diffraction pattern on the surface developed from PDMS were incubated in solutions of the polyelectrolytes. After repeating the process to achieve the desired number of layers of polyelectrolytes, the "inked" stamps were then brought into contact with microscope slides that were cut to desired dimensions. Once printed, the resulting gratings were analyzed using atomic force microscopy (AFM).

Three different polyelectrolyte solutions were used to create diffraction gratings of varying thickness. All polyelectrolytes were purchased from Aldrich and used without further purification. A 2 mg/ml aqueous solution of poly(styrene sulfonic acid sodium salt) (PSS) (MW= 70000), the anionic polyelectrolyte, was made by

Figure 2.1: Optical image of acrylic template used to form PDMS stamps (image size 326.4×244.8 μm)

dissolving the solid polyelectrolyte in Millipore water (18 MΩcm^{-1}). Poly(diallyl dimethylammonium chloride) (PDAC) (MW = 100000-200000, 20% wt in water), the cationic polyelectrolyte, was diluted 62x in Millipore water. For some experiments, solid NaCl was added to the PSS and PDAC. A 4 mg/ml aqueous solution of poly(allyl amine hydrochloride) (PAH) (MW = 70000) was also prepared in Millipore water. The pH of the PAH solution was adjusted to 7.5 using NaOH. PAH is used to facilitate optimum interaction between the polyelectrolyte multilayers and the PDMS[25]. This should help make the PDAC/glass interaction more favorable than the PAH/PDMS interaction. figure 2.2 shows the structures of each of the polyelectrolytes used.

The PDMS stamps were placed in polyelectrolyte solutions ('inking') for 14 minute intervals. The stamp was first incubated in PAH. The sample was then removed from the solution, shaken in a vial of Millipore water for one minute, and incubated in the next polyelectrolyte solution.. The stamp was sequentially incubated in PSS and PDAC until the desired number of layers were accumulated. The stamp was then rinsed one more time in Millipore water, then partially dried under
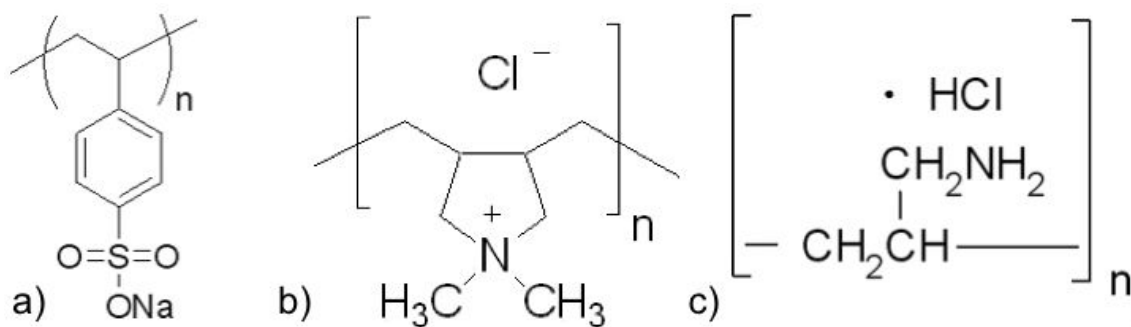
Figure 2.2: Stuctures of polymeric materials used in this study a) PSS b) PDAC c)PAH

a stream of nitrogen. The stamps could be reused multiple times, though after each use they were cleaned by sonicating in a 1:1 mixture of ethanol and water, followed by having their surface peeled with transparent tape to remove contaminants.

Once dried, the stamps were placed on the glass substrates. Light pressure was applied for approximately 30 seconds. The stamps were allowed to rest on the surface for another 15 minutes. Once the stamps were removed the glass substrates were visually inspected for transfer of the patterned polyelectrolytes. Those that showed transfer of the diffraction grating were further characterized by AFM.

2.1.2 Measurement of diffraction intensity

The diffraction intensity was measured using a home made DBS, a schematic of which is shown in figure 2.3. Laser light was focused onto the portion of the sample that yielded the largest diffraction intensity. The prism was attached to the glass microscope slide on the opposite side to the polyelectrolyte grating using an index matching fluid (Richard-Allan Scientific, n=1.5150) . The angle of the incoming laser light was sharp enough such that total internal reflection occurred at the grating. The third order diffraction spot was then focused onto a photodetector (New Focus Large-Area Visible Photoreciever, Model 2031). The diffraction intensity, measured in volts, was recorded using a software routine written in LabView. The routine used is provided in Appendix A.
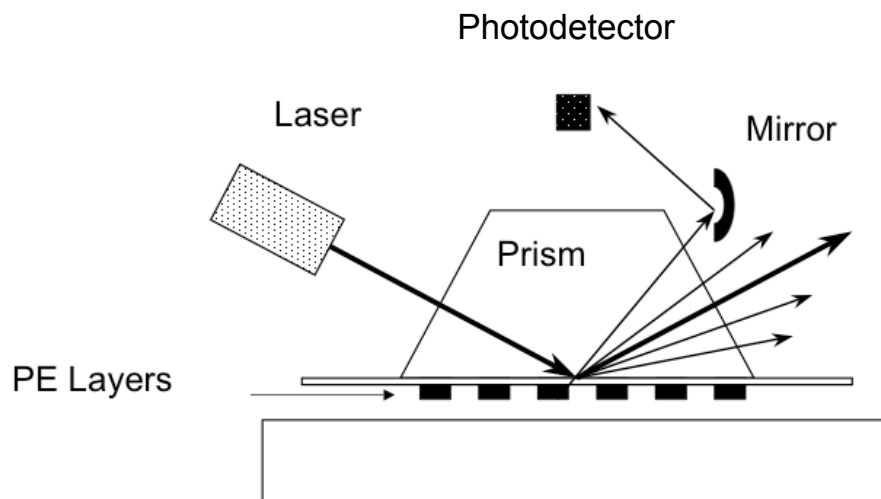
Figure 2.3: Schematic illustration of the DBS system used in these measurements. The grating is made from polyelectrolyte (PE) multilayers.

2.1.3 Varying refractive index of polyelectrolyte diffraction gratings

It has been shown that gold nanoparticles stabilized using 4-dimethyl aminopyridine (DMAP) incorporate readily into polyelectrolyte multilayers [27]. When DMAP is put into aqueous solution, electron rearrangement occurs in the pyridine ring to form the charged species shown in figure 2.4 [27]. The DMAP stabilized gold nanoparticles appear positively charged under the conditions used in these experiments (figure 2.5 This positive charge allows for a favorable interaction with the highly charged polyelectrolytes.
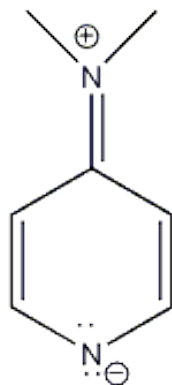
Figure 2.4: Structure of DMAP in aqueous solution

The DMAP stabilized gold nanoparticles were synthesized according to the method described by Gittins and Caruso [26]. An aliquot of 25mM tetraoctylammonium bromide (TOAB) was added to 30 mL of 30 mM $HAuCl_4$ in toluene. Next, 25 mL of 0.4 M sodium borohydride (Na_2BH_4) was added to this mixture. After the solution was stirred for 30 minutes, it was washed three times with 0.1 M sulfuric acid (H_2SO_4), 0.1M sodium hydroxide (NaOH), and water. The solution was then dried over sodium sulfate ($NaSO_4$). A 10 ml aliquot of 0.1 M aqueous DMAP was then added to a 10 ml aliquot of gold nanoparticle solution. The dark purple colour that was initially associated with the organic phase moved to the aqueous layer. We associated this colour change with the nanoparticles undergoing a phase transfer from the organic to the aqueous phase. The aqueous phase was then separated and collected. The DMAP stabilized gold nanoparticles were characterized by transmission electron microscopy (TEM), and UV-Vis absorption spectroscopy.

Polyelectrolyte multilayer gratings were incubated in concentrated DMAP-gold nanoparticle solutions for intervals of approximately 5 minutes. After each time interval, the grating was rinsed in Millipore water, and dried using a stream of N_2(g). The grating was then imaged using AFM. After characterization by AFM the diffraction intensity was determined using the experimental design outlined in figure 2.3.
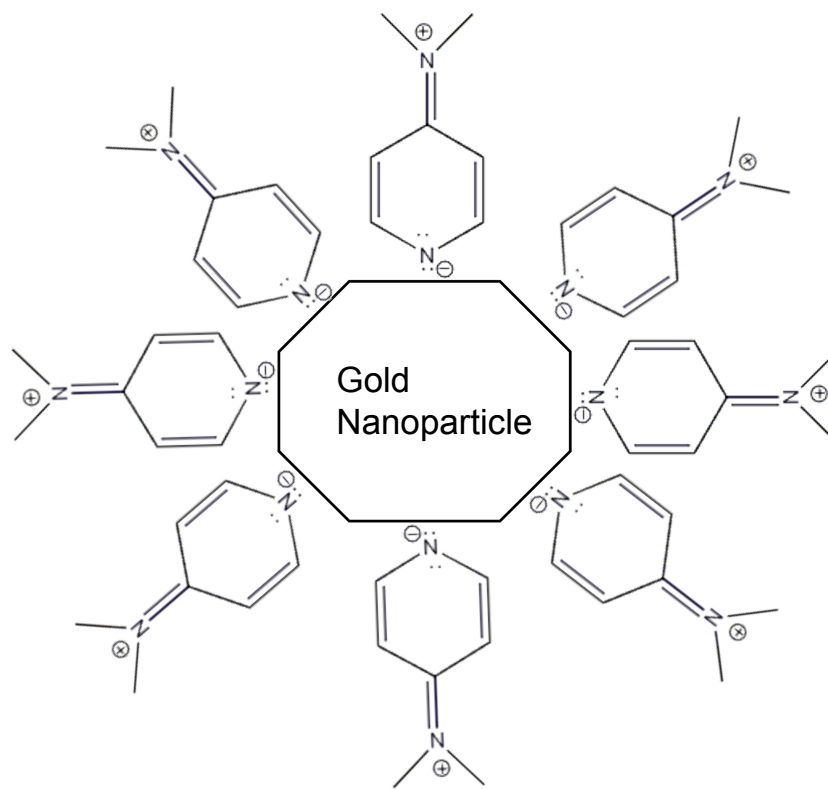
Figure 2.5: A simplified depiction of DMAP stabilized gold nanoparticles. The orientation of the DMAP on the surface causes the complex to appear positively charged.

2.2 Results and Discussion

2.2.1 Theoretical relationship between observed diffraction intensity and grating properties

Before developing and testing the multilayer gratings, we investigated the expected mathematical relationships between the observed diffraction intensity and the grating properties. Equation 1.2 describes the diffraction efficiency of a VPH grating, which, as proposed in Chapter 1, can be used to describe the gratings in this research. The equation, however, is not the easiest to interpret. To simplify it we apply a Taylor

expansion. The general form of a Taylor expansion is

$$\sin x \approx x - \frac{x^3}{3!} + \frac{x^5}{5!} \dots \tag{2.1}$$

Knowing that

$$\sin^2 x = (\sin x)^2 \tag{2.2}$$

The general expansion becomes

$$\sin^2 x \approx (x - \frac{x^3}{3!} + \frac{x^5}{5!} \dots)^2 \tag{2.3}$$

$$\sin^2 x \approx x^2 - \frac{2x^4}{3!} + \frac{x^6}{36} \dots \tag{2.4}$$

For equation 2.4 , we can define $x = \frac{\pi \Delta n d}{\lambda \cos \alpha}$, and assuming $\pi \Delta n d < \lambda \cos \alpha$, this results in $x \approx 0$ allowing us to discard all except the first term in the Taylor expansion.

$$\sin^2 x \approx x^2 \tag{2.5}$$

Substituting for x gives

$$\sin^2 \frac{\pi \Delta n d}{\lambda \cos \alpha} = (\frac{\pi \Delta n d}{\lambda \cos \alpha})^2 \tag{2.6}$$

The diffraction efficiency can now be expressed as quadratically dependent on Δn and d.

$$\eta = (\frac{\pi \Delta n d}{\lambda \cos \alpha})^2 \tag{2.7}$$

To ensure that the assumption that $\pi \Delta n d < \lambda \cos \alpha$ is valid, a simple calculation was performed. Diffraction efficiency, as described by equation 1.2 is graphed against grating thickness and difference in refractive index and is plotted in figures 2.6 and 2.7 . The wavelength of light used is 632 nm, and α is approximated to be $\frac{\pi}{6}$ radians. These values were chosen as they describe the range of values that will be used in the experiment. Varying the thickness of the polyelectrolytes could vary the grating thickness between 0 and 150 nm. The refractive index of polyelectrolyte multilayers was reported to be approximately 1.50 [29] and the surrounding medium is either water (n=1.3), or air (n=1). The plots were then fit to quadratic functions. As can be seen in Figure 2.6 and 2.7 the quadratic relationship holds over the range of thickness and refractive indices being considered. Equation 1.1 describes diffraction efficiency

17
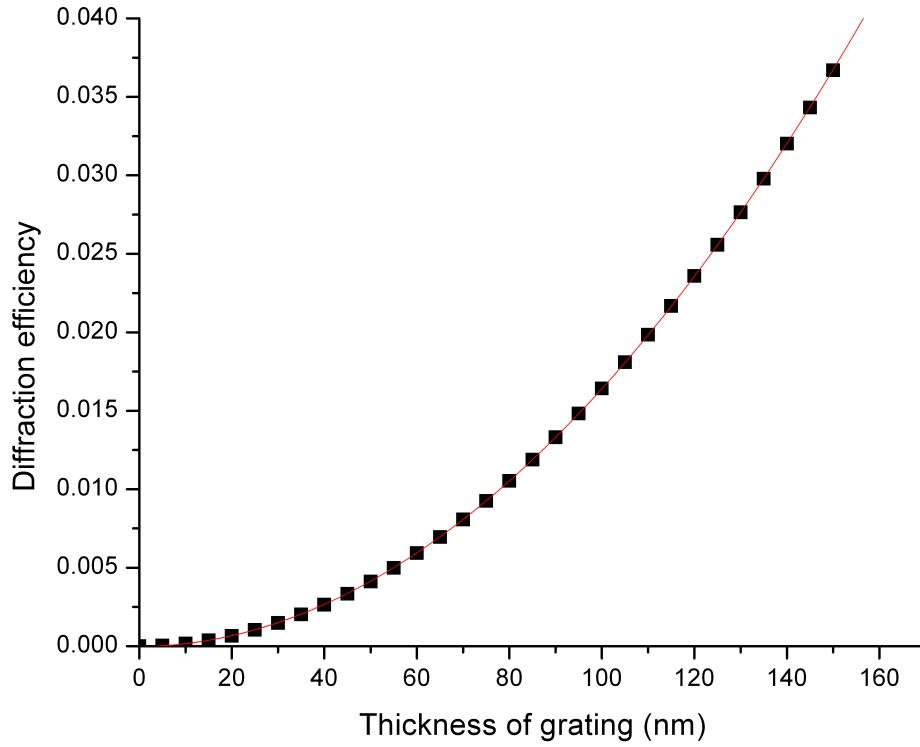
Figure 2.6: Plot showing diffraction efficiency, a dimensionless quantity, as a function of grating thickness. The solid points are calculated from equation 1.2 (λ=634 nm, $\alpha = 30^o, \Delta\text{n}$=0.33). The curve is a second order polynomial fit ($y = yo + ax + bx^2$).

as the ratio of the intensity of the observed diffraction spot over the intensity of the output of the laser. Assuming that any variation in output intensity is small relative to the changes in diffraction intensity caused by the changes in the system, we can say that the experimentally observed diffraction intensity is proportional to the diffraction efficiency. We, therefore, expect the diffraction intensity to vary as the square of the thickness of the diffraction grating and Δn. Should the experimentally derived relationship between diffraction intensity and grating thickness, and Δn be quadratic in nature, we can say that the system is well described by equation 1.2 and has properties that are similar to volume-phase holograms.

18
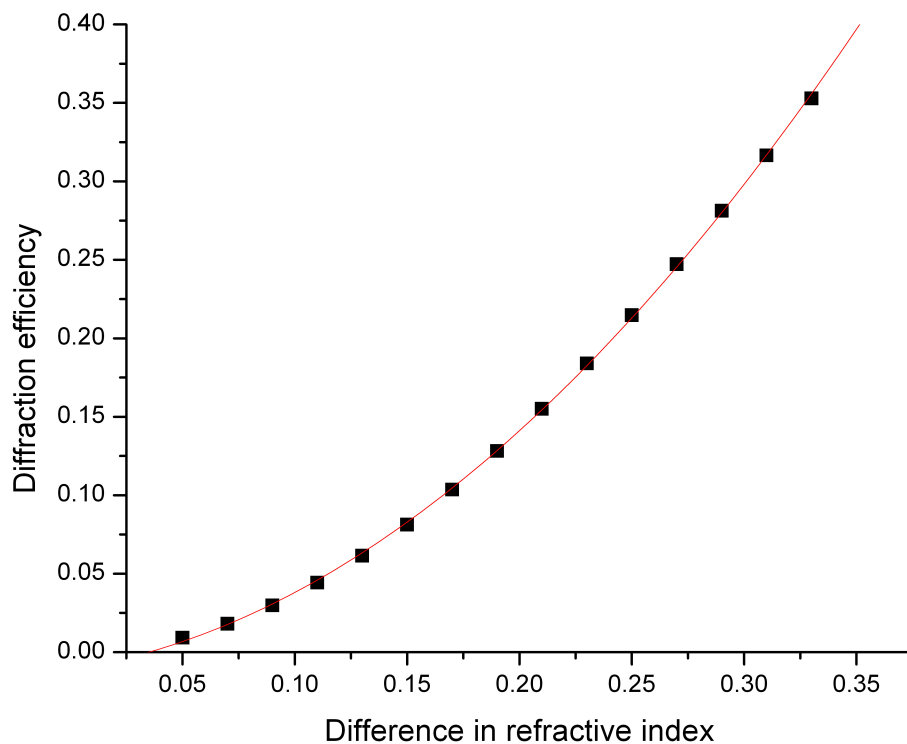
Figure 2.7: Plot showing diffraction efficiency, a dimensionless quantity, as a function of difference in refractive index. The solid points are calculated from equation 1.2 (λ=634 nm, α = 30°, d=65 nm). The curve is a second order polynomial fit ($y = yo + ax + bx^2$).

The DBS used in these experiments relies on total internal reflection illumination. This results in a maximum probe depth, which means that once the sample thickness has reached a certain value, further increases will not change the diffraction signal. The maximum probe depth can be approximated by determining the decay length of the evanescent wave (I_z) that results from total internal reflection. This intensity of the wave decreases as distance (z) from the glass - air or glass-water interface according to [30]:

$$I_z = I_0(\frac{-z}{d})$$

(2.8)

19

Where I_0 is the incident intensity, and d is the decay distance and is given by

$$d = \frac{\lambda_0}{2\pi} |n_2^2 \sin^2 \theta - n_1^2|^{-0.5} \qquad (2.9)$$

Assigning the cut off intensity of the evanescent wave (the value where I_z is negligible) to

$$\frac{I_z}{I_0} = e^{-1} \qquad (2.10)$$

We find that I_z becomes negligible when z =d. The calculated maximum depth that the wave can probe for our system is calculated to be 153 nm. Therefore, the simplification of equation 1.2 by performing a Taylor expansion to yield equation 2.7 adequately describes the dependence of the observed diffraction intensity to the grating thickness. Note this also sets an upper limit on the range of experimental thicknesses, which can be used in this study. The total internal reflection setup should not limit the utility of the sensor as most biomolecules are less than 153 nm in any given dimension.

2.2.2 Diffraction intensity as a function of grating thickness

Varying the number of layers of polyelectrolyte used and the salt concentration of the polyelectrolyte solutions the thickness of the diffraction gratings fabricated by microcontact printing of polyelectrolyte multilayers was controlled. The height of each diffraction grating was obtained from AFM images of the sample. Typically, five high quality images of the surface were collected for each sample. Figure 2.8 a) is an AFM image of a sample produced from nine PSS/PDAC bilayers (note, we define a bilayer of polyelectrolyte as one cationic and one anionic layer of polyelectrolyte). Ten cross-sections of each image were taken, with each cross-section containing approximately 512 points (figure 2.8 b). The cross-sections were then compiled to create a histogram of grating heights. The histograms consisted of two peaks, one associated with the surface of the glass, and the other associated with height of the multilayers (figure 2.8 c). A Gaussian curve was used to fit the histogram, and the peak values were subtracted from one another to obtain the average thickness of the
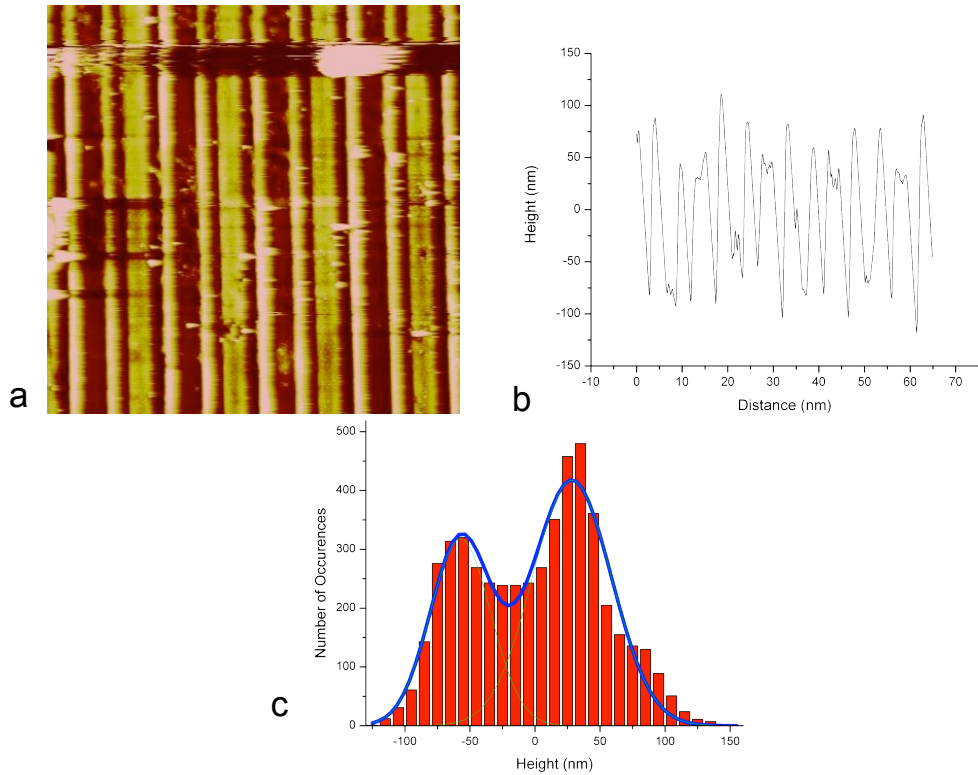
Figure 2.8: a) An AFM image of a diffraction grating formed from nine PSS/PDAC bilayers (65×65 μm) b) Cross-section of AFM image a. c) Histogram compiled from 50 cross-sections of sample shown in a.

film. The uncertainties were determined from the standard deviation of the Gaussian curves.

Initially, gratings were prepared using unfiltered solutions of polyelectrolyte. AFM images of the diffraction gratings revealed small (typically 10 nm in diameter) dots over the entire surface (figure 2.9 a). We hypothesize that the dots were aggregates of polyelectrolyte resulting from a double layer interaction facilitated by the salt in solution. Because of the high charge density of polyelectrolytes, we expect that as salt is added, the double layer effect can allow the polyelectrolytes to fold on themselves, and interact with one another. This interaction, which would occur while the polyelectrolytes are still in solution, would result in the aggregates that
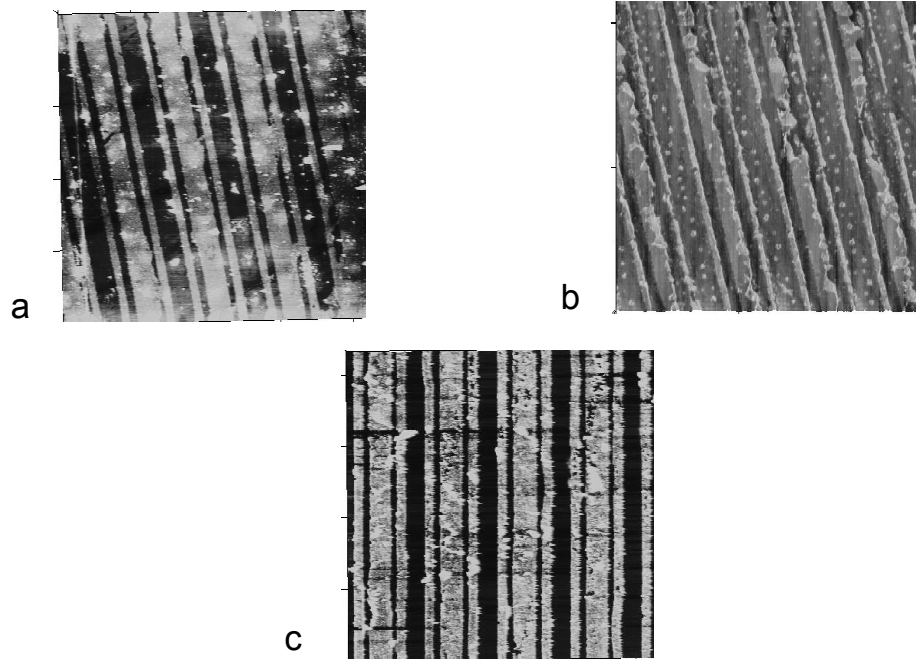
Figure 2.9: Polyelectrolyte multilayers patterned to form diffraction gratings. a) Unfiltered polyelectrolyte solutions used, b) Filtered polyelectrolyte solutions used, c) Polyelectrolyte solution is unfiltered and contains no salt. Each image 65×65 μm

are observed.

Since the presence of the aggregated material led to rough gratings which were somewhat difficult to characterize in the AFM, efforts were made to remove the aggregates. To minimize this problem, diffraction gratings were made from polyelectrolyte solutions that had been passed through a 0.22 μm filter, and from polyelectrolyte solutions without salt. The aggregates were no longer observed in the AFM images of these samples, figures 2.9 b) and 2.9 c) respectively. All future gratings prepared with salt were filtered to remove the aggregated polymer.

A set of polyelectrolyte diffraction gratings of well defined thicknesses were pre-

pared. To achieve a wide range of grating thicknesses a varying number of bilayers of polyelectrolytes and different salt concentration were used. Polyelectrolyte solutions were prepared with final NaCl concentrations of 0, 0.2, 0.4, 0.6, and 0.8 M. We observed that the relationship between the salt concentration, the number of layers and the observed thickness does not follow any obvious systematic trend. We believe this variability, observed in table 2.1, is due in part from the marginally larger affinity of the polyelectrolyte multilayers for the glass when compared to the PDMS. PAH is the layer that is immediately adjacent to the PDMS, while PDAC is the layer that is immediately adjacent to the glass substrate. For microcontact printing to be effective, the PDAC/glass interaction needs to be larger than the PAH/PDMS interaction. This is, of course, how the multilayer is engineered. However, the polyelectrolyte multilayers form an amorphous thin film [24]. This means that the layer adjacent to the PDMS is a mixture, largely of PAH, but with significant amounts of PSS and PDAC, and the layer adjacent to the glass is a mixture of PDAC and PSS. This will cause the difference in affinity of the multilayers towards the glass substrate to be similar to that of the PDMS. This difference is therefore smaller than if the substrate and the stamp were made from two very different materials, and causes the variability in results observed in the microcontact printing.

The experimentally determined relationship between thickness of the diffraction grating and the observed diffraction intensity, Figure 2.10, follows a quadratic relationship. This result agrees with the theoretically derived result (Figure 2.6). This suggests that the VPH equations can be used as a successful model for this system.

This means that the mechanism of diffraction occurring in the diffraction gratings is the same as that of Volume-phase holograms. As light enters into the diffraction grating area, a few of the wave trains pass through areas of air, while others will enter the area of polyelectrolyte. Given the difference between the refractive indices of the two media, the wave trains will no longer travel at the same velocity. When they re-emerge they will be out of phase with one another. The extent that they are out of phase will determine the intensity of the observed diffraction. Since the refractive index is constant, the only way to control the difference in phase is by

Table 2.1: The heights, number of bilayers, and concentration of NaCl for diffraction gratings used to determine the dependence of intensity of a given diffraction spot on thickness of the grating.

Entry	[NaCl] (M)	Number of bilayers	Height (nm)
1	0.4	9	51±6
2	0.4	9	65±6
3	0.8	7	71±6
4	0.8	7	84±14
5	0.6	7	98±3
6	0.8	9	138±3

changing the path length that the light must travel. The optical path length is given by the thickness of the grating. Therefore, the thickness of the grating will control the degree that the wave trains are out of phase with one another.

This gives new insight to some previously reported results. For example in the work presented by Fiori and Paige [6], a grating made from mouse IgG was degraded by the enzyme trypsin as a function of time. The diffraction intensity was found to decay exponentially as a function of time. The observed diffraction intensity decreased to 20% of its original value after 15 minutes of incubation. Now, we can translate the observed diffraction intensity into a grating thickness. The diffraction intensity will still scale exponentially with thickness of the grating. The rate of decay of the exponential will, however, be more rapid. This would mean that after 15 minutes, the resulting grating should be approximately 4% of its original thickness. This reinforces the suggested first order mechanism suggested by Fiori and Paige [6]. Since the mouse IgG is immobilized on a solid surface, we would not expect
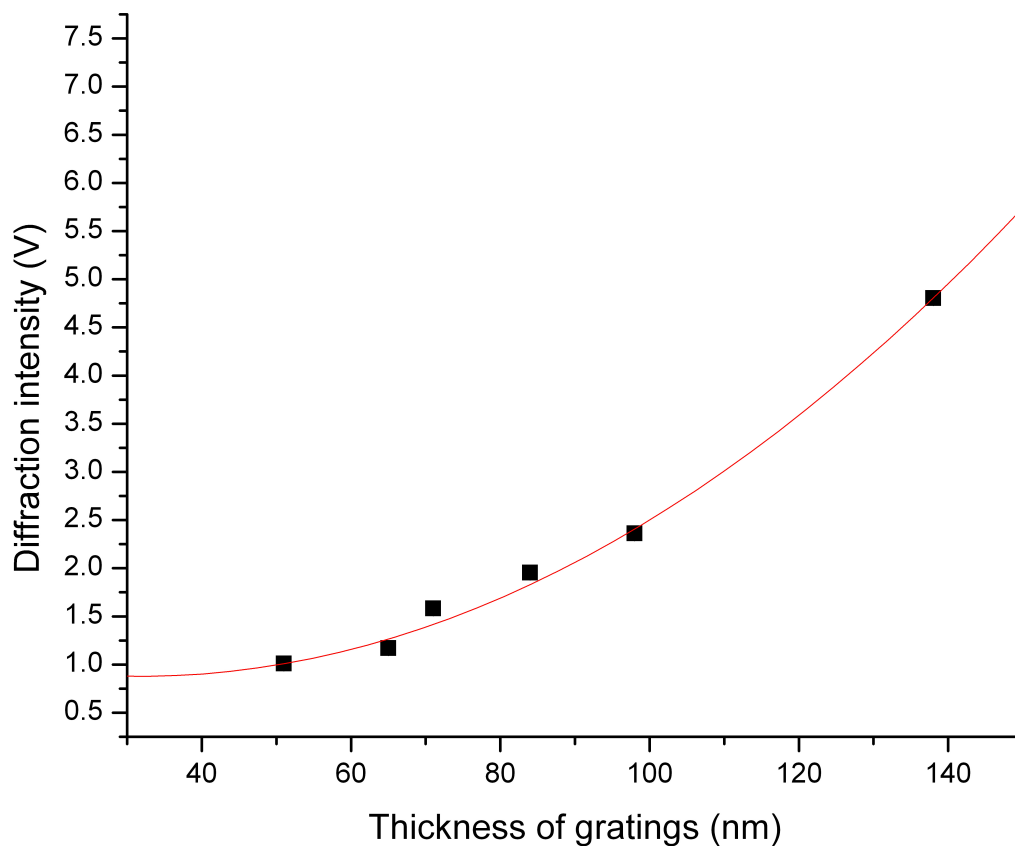
Figure 2.10: Plot of experimentally measured diffraction intensity as a function of grating thickness. The line is a second order polynomial fit.

the concentration of the IgG to play a role in the mechanism of the reaction. We now have access to real kinetic parameters that are involved in this reaction. A similar analysis will be performed on the work by Goh and coworkers[3] on real time monitoring of the binding of rabbit and mouse anti-IgG to their complimentary immunoglobulins in Chapter 3.
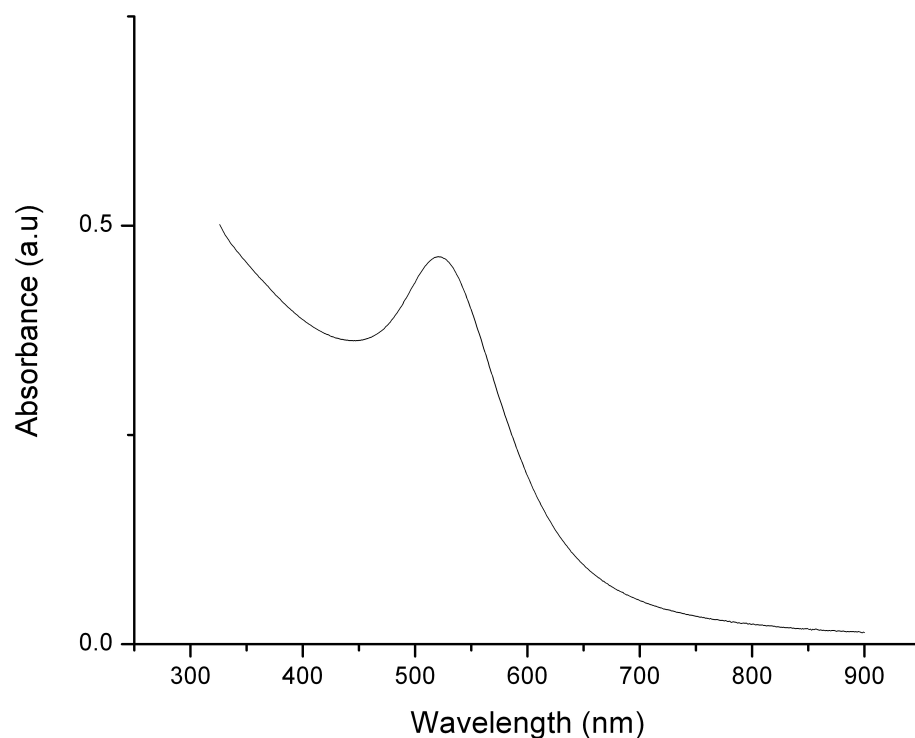
Figure 2.11: UV absorbance spectra of DMAP stabilized gold nanoparticles

2.2.3 Diffraction intensity as a function of grating refractive index

The DMAP stabilized gold nanoparticles were characterized by UV-Vis absorption spectroscopy and TEM to qualitatively determine the size and distribution of the nanoparticles. Figure 2.11 shows the UV absorbance spectra of the DMAP stabilized gold nanoparticles. Figure 2.12 shows a TEM image of the DMAP stabilized gold nanoparticles. From the position of the absorbance peak of the nanoparticles, as well as the TEM image we see that the synthesized nanoparticles were relatively monodisperse with a size of approximately 6 nm.

As mentioned earlier, to adjust the refractive index of the polyelectrolyte grat-

26

ings, well-characterized samples were incubated in a concentrated aqueous solution of DMAP stabilized gold nanoparticles. Figure 2.13 shows that as the grating was exposed to the aqueous nanoparticle solution for a longer period of time, the concentration of the nanoparticles on the surface increases. The observed dots are truly nanoparticles due to their size, and their absence from other samples that were not placed in the aqueous DMAP-gold nanoparticle solution. We also notice that there are no real changes in the diffraction grating. The thickness, and spacing of the grating are approximately the same for all these images.

We note that for exposure times above 30 minutes, the diffraction intensity rapidly decreases. Characterization of these samples by AFM shows poorly defined grating structure. This is a result of the polyelectrolyte multilayers being removed by exposure to the solution (figure 2.14).

After the nanoparticle doped gratings were characterized by AFM, the intensity of the diffaction pattern was measured in the DBS. The diffraction intensity measured from the incubated gratings increased linearly with nanoparticle incubation time (figure 2.15). If one assumes that the variable Δn in equation 2.7 is directly proportional to the incubation time, this result is in good agreement with that expected for the VPH gratings.

Given that the exposed surface of polyelectrolyte is amorphous in nature, the surface of the polyelectrolyte will be a mixture of the PSS and PDAC. We therefore assume that the net surface charge that the polyelectrolyte multilayers exhibit in the bulk is zero. Let us first assume a uniform concentration of the nanoparticles throughout the solution. Since the nanoparticle solution is quite concentrated, it is logical to assume that the number of available sites on the surface will control the maximum number of nanoparticles that can be adsorbed. With such large charges in the multilayers, it is also reasonable to assume that the effect of the charge of DMAP will be masked and not affect the ability of a subsequent nanoparticle from adsorbing. Combined this makes the concentration of nanoparticles on the surface a function of time only. This system now can be modeled by the Langmuir Isotherm,

$$\Phi = \frac{bt}{1 + bt} \tag{2.11}$$

Where Φ is the fractional surface coverage, b is a ratio of the adsorption rate constant over the desorption rate constant, and t is the time allowed for adsorption. Figure 2.16 shows a typical Langmuir isotherm. This curve is initially linear with a steep slope. It then approaches saturation and plateaus. Given the relatively short incubation period [27] it is reasonable to assume that adsorption is occurring in the first region of this curve.

The second assumption required for our data to fit within the expected result from equation 2.7 is a linear dependence in change in refractive index with changing nanoparticle loading. With both of these assumptions we should see a quadratic relationship. However, since the nanoparticles are small relative to the grating thickness, we can expect scattering of the light between the particles. In general, for a grating, the intensity of the scattered light scales quadratically with its thickness according to equation 2.7. Nevertheless, when a certain number of particles are loaded onto the grating, the situation is more complicated. When the radius of the particles is smaller than the width of the pattern stripes, the spheres tend to organize randomly within each stripe of the diffraction grating. Thus the effect is an ensemble of spheres which are only partially ordered when looking at the larger surface. In this case, as the number of beads increases, the scattered intensity cannot grow quadratically, as it would happen for a perfectly ordered grating. On the contrary, when the sphere radius is more or less equal to the stripe width, the beads tend to be perfectly aligned, with the result of a constructive interference in the scattered light, the intensity of which scales quadratically. This result, therefore, does not contradict the results expected from equation 2.7. It would be beneficial, however, to be able to view the diffraction intensity purely as a function of refractive index, without having to worry about the scattering effects.

2.3 Conclusions

The diffraction intensity was theoretically determined to follow a quadratic dependence on grating thickness (optical path length) and refractive index modulation

within the limits of the DBS system. Using polyelectrolyte multilayers, a series of gratings of varying thickness were developed, and the diffraction intensity as a function of grating thickness was found to follow a quadratic relationship in accordance to theory. The polyelectrolyte gratings were then loaded with DMAP stabilized gold nanoparticles to vary the refractive index of the gratings. The relationship between the time allotted for nanoparticle loading and observed diffraction intensity follows a linear relationship. This variation from theory is attributed to scattering of light off of the nanoparticles.
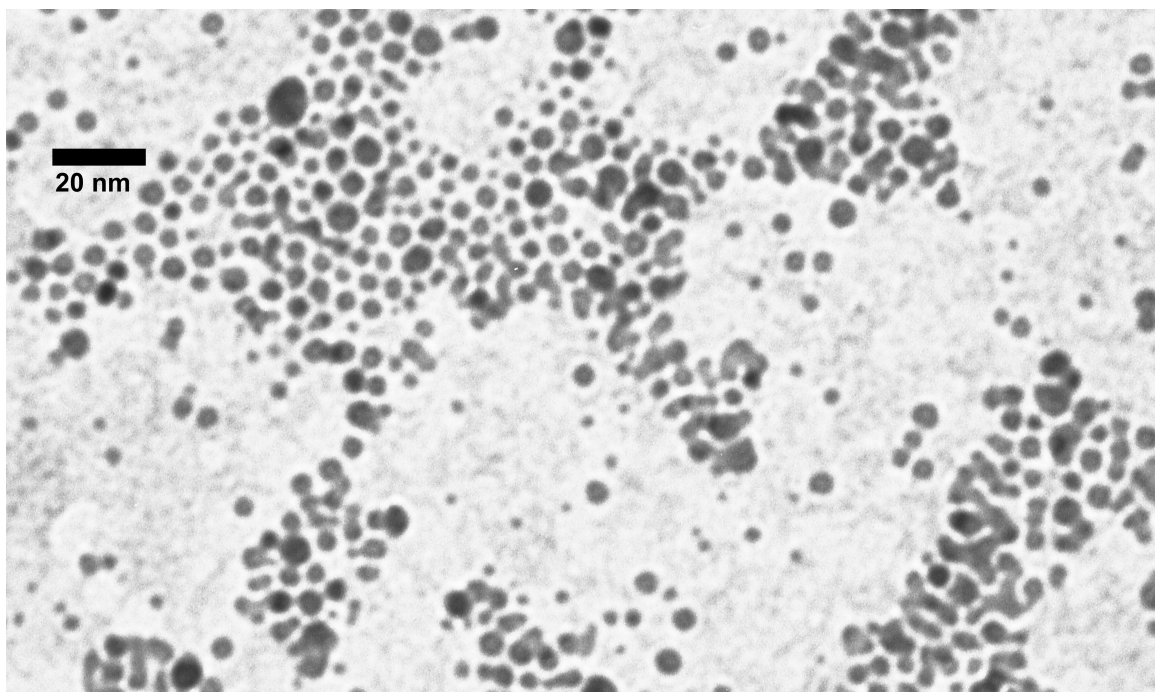
Figure 2.12: Transmission electron microscope image of DMAP stabilized gold nanoparticles
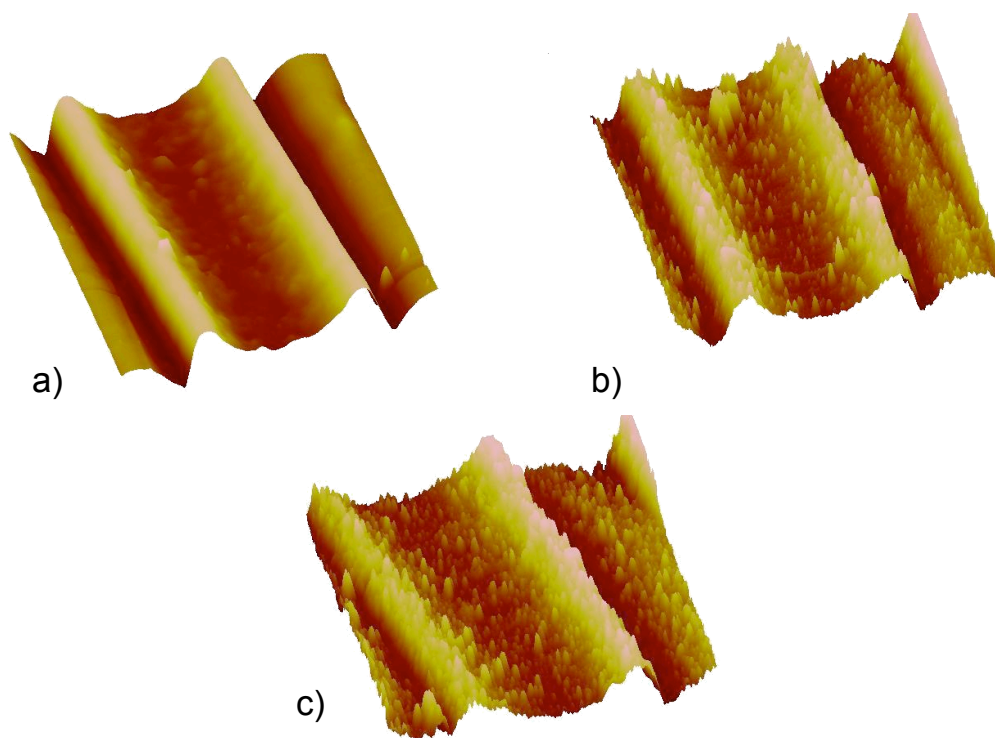
Figure 2.13: Tapping mode AFM images of a polyelectrolyte grating after a) 0 b)11 c) 22 minutes of incubation in aqueous gold nanoparticle solution. Each image 6×6 μm.
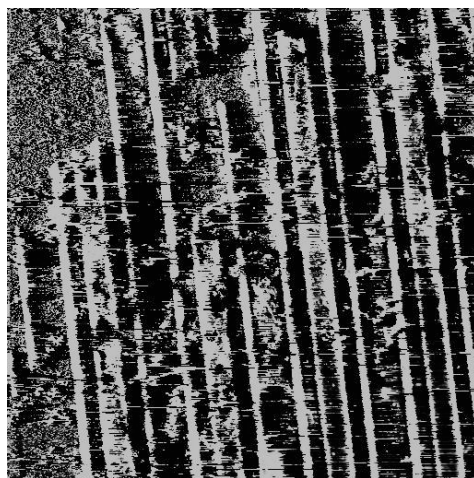
a   b

Figure 2.14: Polyelectrolyte diffraction gratings after submersion in aqueous nanoparticle solution for a) 22 minutes b) 35 minutes
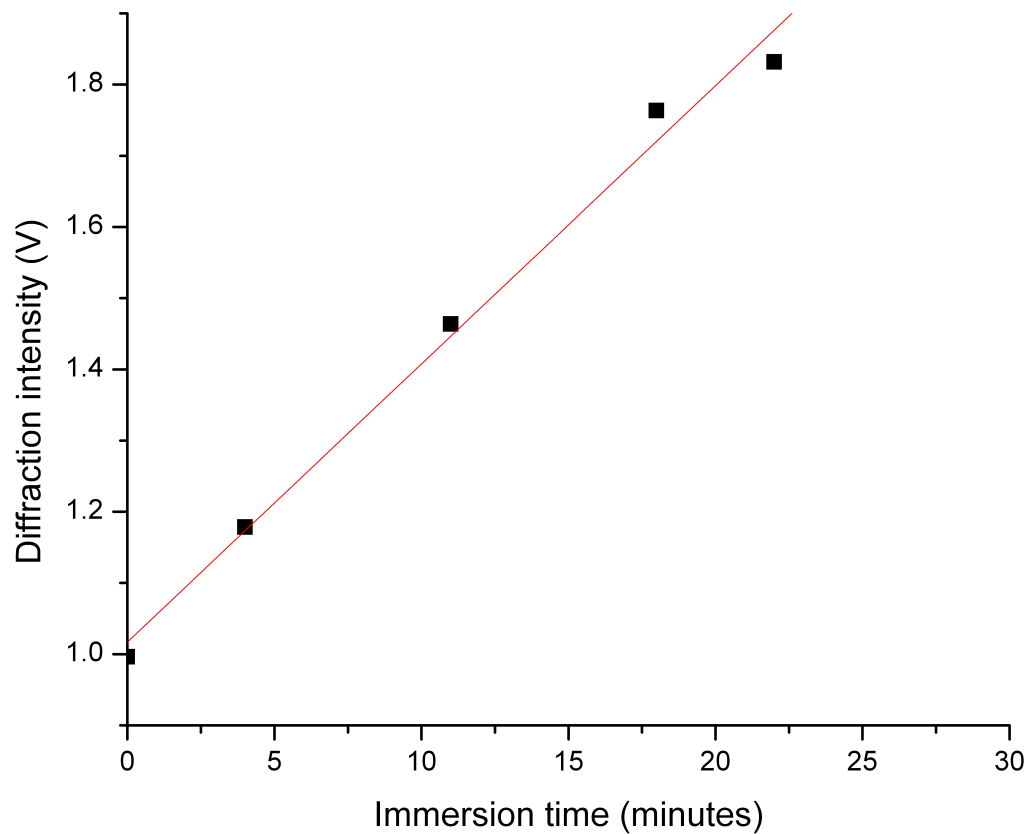
Figure 2.15: Plot of diffraction intensity as a function of the time the diffraction grating was immersed in the gold nanoparticle solution. The line is a linear fit to the data.
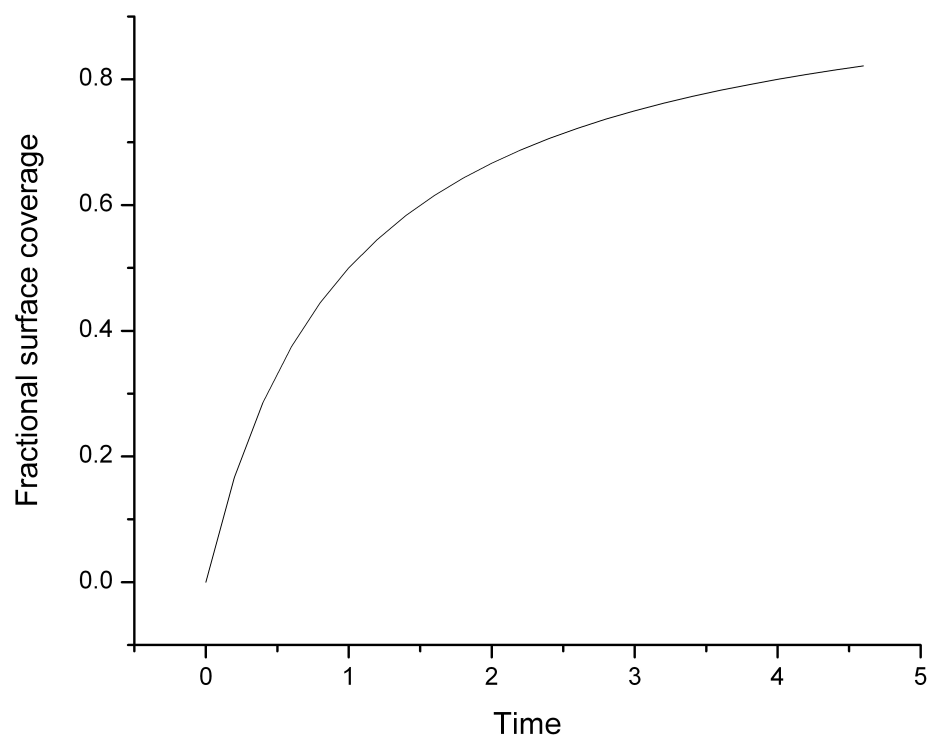
Figure 2.16: Generalized Langmuir isotherm

CHAPTER 3

CHARACTERIZING THE EFFECT OF PARTICLE LOADING ON DIFFRACTION EFFICIENCY

3.1 Materials and methods

3.1.1 The system

DBS systems operate by monitoring the change in intensity of a diffraction spot as analyte molecules bind to a functionalized grating. So far we have described how the diffraction intensity varies according to the properties of the grating. The second portion of this research involves determining how particle loading effects the observed diffraction intensity. Since recent publications have focused on quantification of analyte, and reaction kinetics on the grating surface[3, 6], we also perform kinetic experiments to relate the observed data to kinetic parameters such as adsorption rate, and extent of particle loading.

For these measurements, we have made use of a commercial DBS, the dotLab^{TM}system (Axela Biosensors Inc., Figure 3.1 [31]). The main benefits of this system over the more simple home-made system described in the previous chapters include integrated fluidics, and an established user interface. Disposable diffraction gratings were made out of the biopolymer avidin printed on a PS substrate (Axela Biosensors Inc.). The analyte particles consisted of 2 μm PS beads that had been functionalized with carboxyl groups (Polysciences). A 50 μL aliquot of the beads was mixed with 5 mL of phosphate buffer solution (pH = 7.4). A new grating was used for each experiment.

Figure 3.1: The Axela dotLab^{TM} system. Reproduced from [31]

Each experiment consisted of a series of steps. First, the sensor surface was rinsed with 500 μL of phosphate buffer solution with 10% Tween v/v (pH=7.4). Tween is a polyethylene based detergent. During this process, the solution was oscillated over the grating surface 10 times. This rinsing was repeated two more times to ensure that any contaminants on the grating surface had been cleaned off. Next, the injection needles that are used to deliver the sample were cleaned with a phosphate buffer solution (pH=7.4). A 60 μL aliquot of phosphate buffer solution (pH=7.4) was then drawn into the sensor, and oscillated over the surface 500 times to remove any Tween detergent left after the washings. After another tip washing, 60 μL of the 2 μm bead solution were drawn into sensor. This solution was left to incubate on the sensor surface for a varying period of time to allow the beads to adsorb onto the grating surface. The incubation times for the PS beads were 350, 860, 1500, 2000, 2800, 4200, and 5400 seconds.

Avidin is known to bind the water-soluble vitamin biotin with the highest affinity known for non-covalent interactions. The isoelectric point of avidin is approximately 10.5, making it negatively charged at the pH used here. Since the PS beads used were carboxylated, they have a net negative charge at a pH of 7.4, and bind to the

avidin grating via electrostatic interactions.

3.1.2 Characterization of the surface particle loading

After the PS beads were allowed to incubate on the grating surface, the sensor was disassembled, and optical microscopy was used to view the surface. Each sensor consisted of 8 independent gratings which were 1.462 mm in diameter. The second and third grating were used for all analysis as these gratings were the least likely to be damaged during the disassembly process. Five optical images of each grating were captured using a Nikon Coolpix digital camera. Before each session, a calibration grid was used to determine magnification scale of the images. An example of an optical image is given in Figure 3.2.
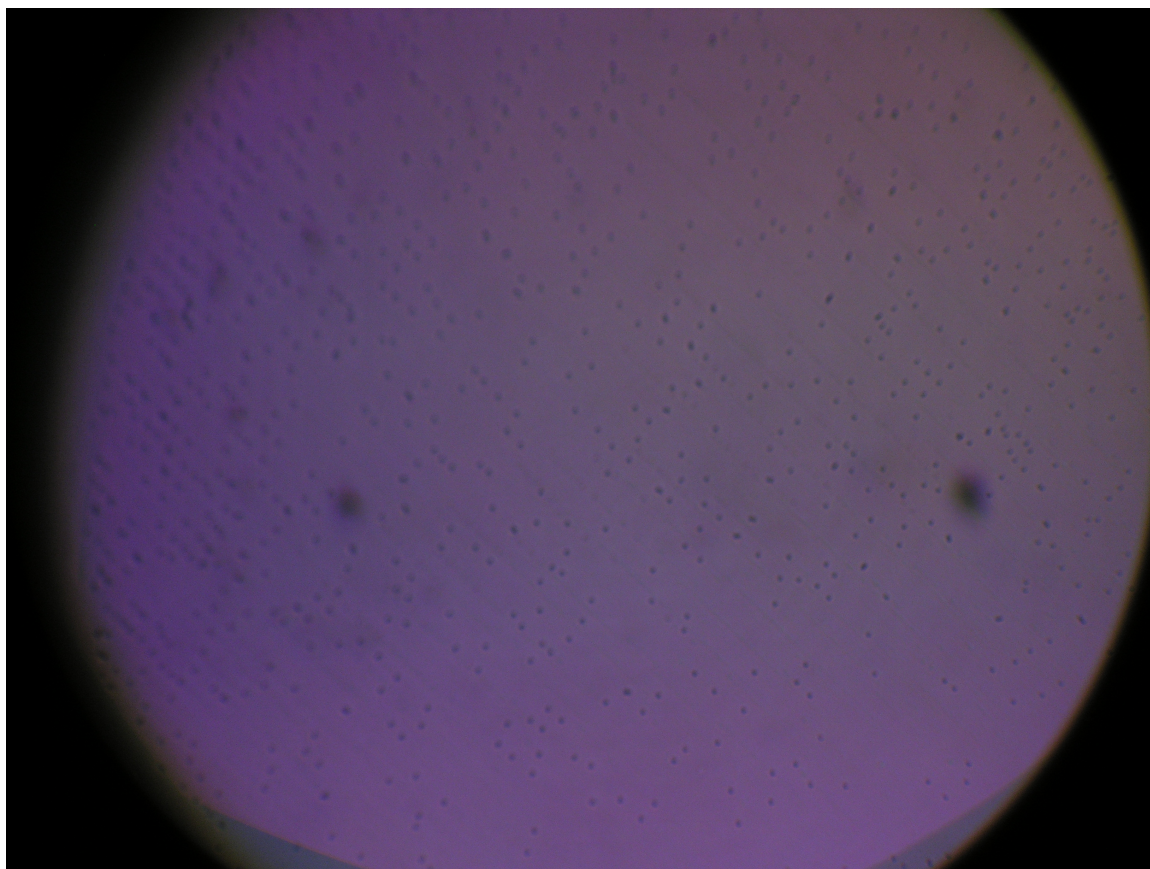
Figure 3.2: Optical microscopy of 2 μm carboxylated PS beads on an avidin grating. Magnification $=20\times$. Viewing area$= .496$ mm^2

The resulting images were processed using ImageJ (NIH). Once the RGB images were converted to 8-bit images, the picture was converted into binary pixels by setting a threshold. The image was then analysed to count all particles (pixels within the threshold) with a size between 36-1000 pixels^2 which translates to particle sizes between 1 and 7 μm. Once the number of particles were counted, the number of particles per area were determined for each surface. This was then averaged, and the total number of particles on the grating was estimated. The observed diffraction intensity was then plotted as a function of the number of particles on the surface.

Another major area of interest is the effect of particle order on the surface on the observed diffraction intensity. We tried to develop a method to quantify the degree of periodicity in the system. To measure this, the following approach was taken: three replicate samples were made with incubation times of 4200 seconds. Optical microscopy was used to image each of these surfaces. Five images were taken of the second and third diffraction grating on the sensor, and the Fourier transform for each image was calculated. The Fourier transform is a linear operator that breaks down an image or function into its frequency components. As can be seen from Figure 3.3, the Fourier transform yielded a series of bright spots in a row. Each of these spots represents the frequency of repetition and associated harmonics. From the intensity of these spots, we can determine the extent that this particular frequency occurs. As the peaks are more intense, the more pronounced that particular frequency is. Any periodicity change will be reflected in the intensity of the peaks. If the particles load in a manner that keeps or increases the periodicity of the grating, then the peaks would be more intense than if they order in a manner that would decrease the periodicity of the grating. The cross section of these peaks were taken, and the intensity of these peaks, were summed and divided by the sum of the intensity of each pixel to reduce errors caused by variations in image size. This was averaged with the Fourier transforms of the other four images to yield a normalized peak intensity. The relative average normalized peak intensity should give insight into the comparative order of the particles in the system.
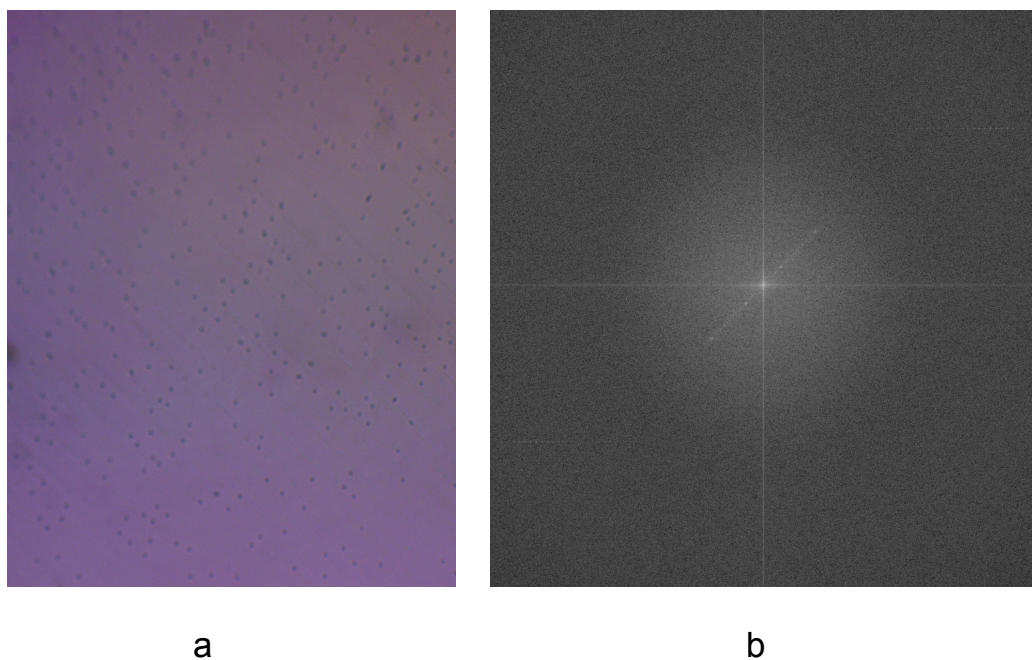
Figure 3.3: a)Optical image of PS beads on an avidin grating - image size 473×303 μm. b) Fourier Transform of a.

3.1.3 Adsorption kinetics

A strength of DBS systems is the potential to probe reaction mechanisms through characterizing the kinetics of biologically important reactions [3, 6]. We show here, for the first time, the use of a DBS system to extract certain reaction parameters in a simple test system, the binding of carboxylated PS beads to an avidin surface. The Axela dotLab system outputs intensity of a diffraction spot as a function of time. The data for each run were then plotted in Origin, and analyzed using Origin's non-linear curve fitting routine. Each data point includes the data for an experiment of the specified duration as well as the data for that time for all experiments of longer duration.

3.2 Results and discussion

3.2.1 Effects of particle loading on the diffraction intensity

Figure 3.4 shows the experimentally determined diffraction intensity as a function of particle loading. We see that as the number of particles on the surface increases, the diffraction intensity also increases, and that the trend is well described by a quadratic relationship. We have already established that this relationship is the behavior predicted for a system following the same mechanism as volume-phase hologram gratings. Assuming that the refractive index of avidin and the polymer spheres are similar, this implies that the particles that are on the surface act to increase the path length of the light. This increase in path length is the cause of the observed increase in diffraction intensity.

It must be noted that this change in path length is not homogeneous over the entire surface. Only areas where the particles have adsorbed onto the surface will have an increased optical path length. We assume that there are three paths that light can travel. The wave trains can reflect off the substrate surface, or travel twice the height of the grating after reflecting off the grating surface, or twice the height of the grating and the particle. Here the difference in path length is equivalent to the path length of one of the wave trains through the higher refractive index medium, and therefore the degree that two wave trains are out of phase is dependent only on the difference in path length.

Since the exposed substrate is constant, we assume that the percentage of light reflecting off the substrate surface will remain constant. The variation, then, comes from the amount of light that can travel the longer particle path length. Given that we established that the more out of phase the wave trains would be, the larger the intensity of diffracted spots, those wave trains that travel the longer path (those where a particle is adsorbed) will be out of phase with the wave trains that reflect off the surface to a greater degree than those that only reflect off the grating. As more particles adsorb onto the surface, a larger percentage of light will travel this
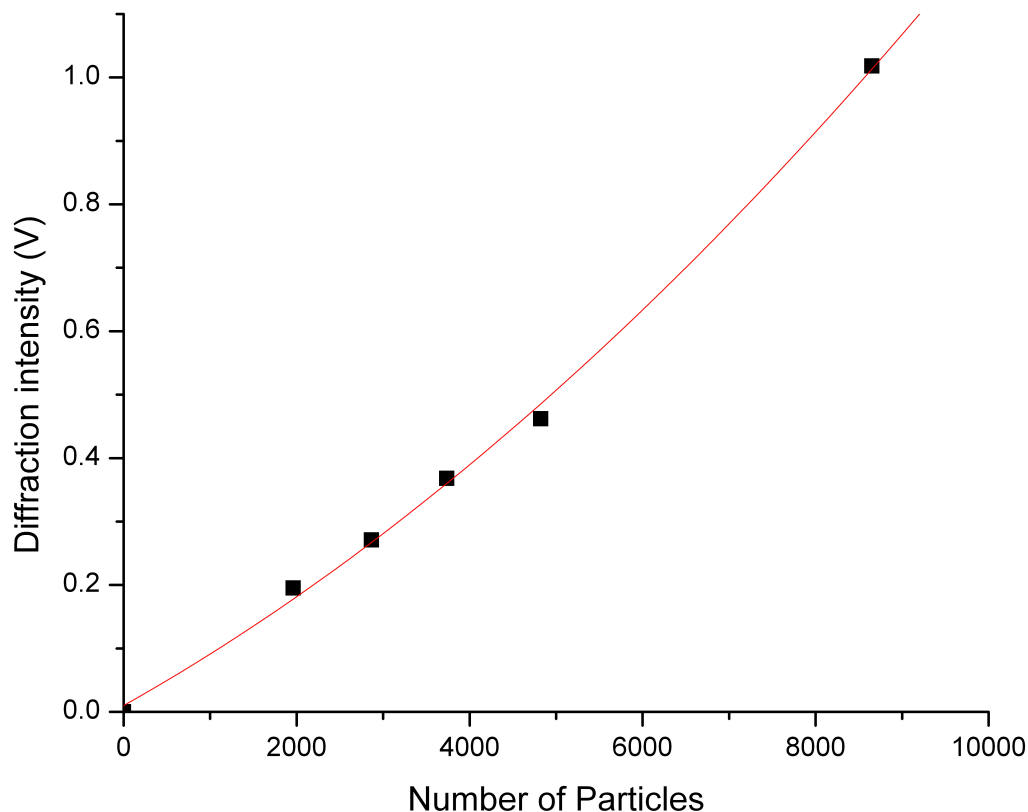
Figure 3.4: Plot showing diffraction intensity as a function of number of particles on the grating surface. The line is a second order polynomial fit to data, $y = 4.173 \times 10^{-9} x^2$.

longer distance and contribute to larger diffraction intensity. If we assume that each of the two thicknesses contributes linearly to the observed diffraction intensity, then the trend observed can also act as the average thickness of the grating.

We can now gain greater insight into results such as the real-time measurements of rabbit and mouse anti-IgG binding to their immunoglobulin reported by Goh and co-workers [3]. Here intensity data were collected as a function of time as anti-IgG binding occurred for various concentrations of anti-IgG solutions. The diffraction intensity scaled exponentially as a function of anti-IgG loading. It should be possible, in the future, for researchers to convert the signal into a surface concentration of

bound material. Using the relationship between diffraction intensity and number of large particles on the surface derived earlier, the diffraction intensity can be translated into number of anti-IgG molecules on the surface. When diffraction intensity is translated into particle loading, we will still see an exponential dependence, but again the slope of this curve will be steeper. This will again yield kinetic parameters of this reaction, which will give insight into the nature of the antigen/antibody interaction.

3.2.2   Effects of particle order

As described earlier, the most obvious cause of variation of the behavior of diffraction intensity as particles are loaded onto a surface compared to that of changing thickness of the grating is caused by the scattering of light by the particles. These scattering effects are expected to be most pronounced as long range order of the particles decreases. We began developing a method to quantify the degree that the particle loading decreases the periodicity of the grating. Time limitations, however, prevented us from completing the development of this method. The observed relationship between the diffraction intensity and the number of particles in this system does follow a quadratic relationship. We expected, then, that any variation in order to be relatively small.

The Fourier transform of the optical image was cropped, and a cross-section is taken of the observed spots (Figure 3.5). An optical image of a bare grating was taken as well. The Fourier transform of that grating did not show any of the characteristic spots. This makes intuitive sense as the diffraction grating is not visible in the optical images at this magnification. Consequently, this shows that any observed spots will be due to the particles mimicking the periodicity of the grating. Meaning, that if the particles had a similar affinity for the substrate surface as the grating surface, we would not expect to see the characteristic spots in the Fourier transform.

Figure 3.6 compares the cross-sections of two Fourier transforms of two different samples. The averaged normalized peak intensity of these samples are $(3.7 \pm 1.1) \times 10^{-6}$ and $(4.1 \pm 1.3) \times 10^{-6}$. The error is one half the standard deviation of the

value that formed the average. Table 3.1 shows the average peak intensity of the six diffraction gratings.

As is clearly visible by the similarity in the size of the peaks in these graphs, and the resulting averages in peak intensity for these, the order of the particles is the same for these samples within the limits of the technique. This is also true of all six diffraction gratings that were investigated for this section.

Table 3.1: List of the average normalized peak intensities for six diffraction gratings.

Entry	Average normalized peak intensity
1	$(6.7 \pm 1.7) \times 10^{-6}$
2	$(3.7 \pm 1.1) \times 10^{-6}$
3	$(3.5 \pm 1.1) \times 10^{-6}$
4	$(4.1 \pm 1.3) \times 10^{-6}$
5	$(6.8 \pm 1.9) \times 10^{-6}$
6	$(4.1 \pm 0.9) \times 10^{-6}$

This experiment can now be repeated with smaller particles to give a wider range of order. Particles that are significantly smaller than the width of the grating have a larger number of possible configurations to load. These smaller particles will have more variability with respect to the location on the grating surface they will load. This will cause a wider range of possible configurations of the particles on the surface, and will result in greater differences in the average peak intensities.

3.2.3 Characterization and modeling of analyte adsorption kinetics

We elucidate here, for the first time, the kinetic parameters of a reaction using the DBS. Knowing that diffraction intensity can be translated directly to the number of particles on the surface, the diffraction intensity of 2 μm PS beads loading onto an avidin grating is measured as a function of time. A single exponential function is used to model this curve. Figure 3.7 shows the diffraction intensity as a function of time.

Given the shape of the curve, as well as the fact that only monolayer coverage was observed using optical microscopy, we initially assumed the system could be described using a Langmuir adsorption isotherm. Figure 2.16 shows a characteristic Langmuir adsorption isotherm curve. Fitting the data with a Langmuir isotherm did not result in curves that closely described the trend exhibited by the data. One of the requirements for Langmuir-type behavior is a rate of adsorption on the same order of magnitude as the rate of desorption. Experiments showed the rate of desorption was found to be orders of magnitude faster than that of adsorption, eliminating Langmuir as a possible model. As an alternative to the Langmuir isotherm, the data were fit with a single exponential function:

$$y = A_1(1 - e^{-kx}) \tag{3.1}$$

Careful analysis of this equation yields a few useful parameters of the observed reaction. The prefactor, A_1, describes the maximum diffraction intensity that can be observed. This will give the maximum number of particles that can be adsorbed onto the surface. Performing the conversion of diffraction intensity to number of particles on the surface from the equation determined in Figure 3.4 gives a maximum particle loading of approximately 34000 particles on the grating surface (20230 particles mm^{-2}). Figure 3.8 shows the rate of adsorption of the grating PS beads as a function of time after translating the diffraction intensity into number of particles on the grating surface.

The absolute value of the coefficient, k, is 7.593×10^{-4} s^{-1} gives insight into the rate of adsorption of the PS beads. It takes $\frac{1}{k}$ (1317) seconds for $\sim 63\%$ of the calculated maximum number of PS beads (~ 21420) to load. Therefore the initial rate of adsorption of the particles is $16.26 \frac{particles}{s}$. Since we have a two reactant system, where once reactant is essentially constant, as it is bound to a surface in the form of a diffraction grating, it is easy to assume that the observed rate of the reaction depends solely on the concentration of the PS beads. Relating this back to the work of Fiori [6] and Goh[3], the rates in each of these systems depend only on the concentration of the Trypsin and anti-mouse IgG respectively. Further work is needed, however, to gain insight into the mechanism of adsorption and the associated kinetics.

3.3   Conclusions

The dependence of diffraction intensity on the degree of particle loading was determined for the system where 2 μm carboxylated PS beads are loaded onto a diffraction grating made from the biopolymer avidin. Using the Axela dotLab^{TM} system this relationship was found to follow a quadratic functional form. A method was developed to quantify the degree of the ordering of the particles. The degree of order for all samples within our system is the same within the detection limits of the technique, which is the expected result given the relationship between diffraction intensity and number of particles on the surface. The kinetics of this system was also investigated, and the extent of particle loading, as well as the rate of adsorption of 2 μm carboxylated PS beads were determined. The maximum loading of these beads was determined to be 20230 particles mm^{-2}. The rate of adsorption of the particles is $16.26 \frac{particles}{s}$.
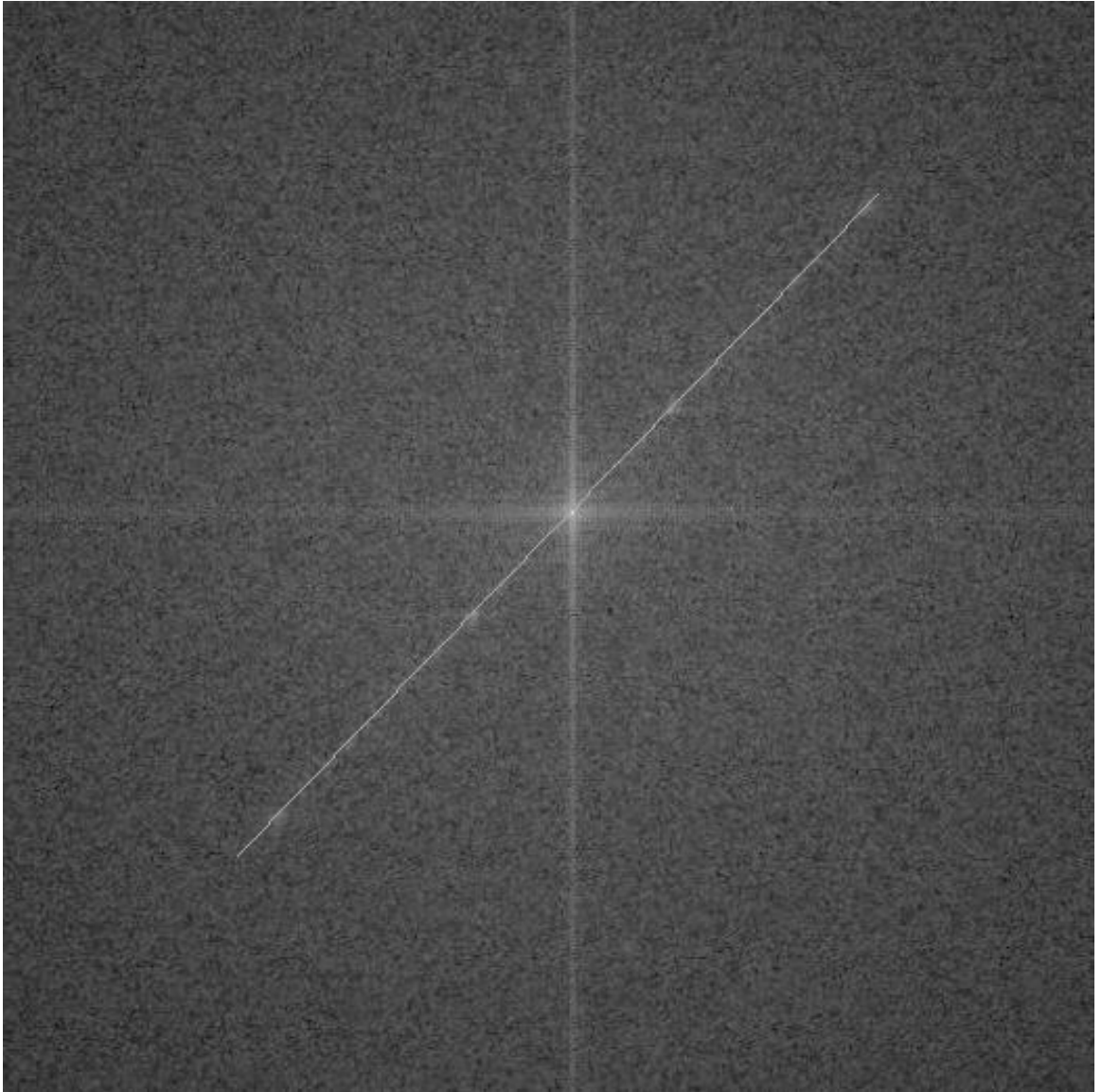
Figure 3.5: Cropped Fourier transform of optical image in figure 3.3. The diagonal line indicates the position of the cross-section.
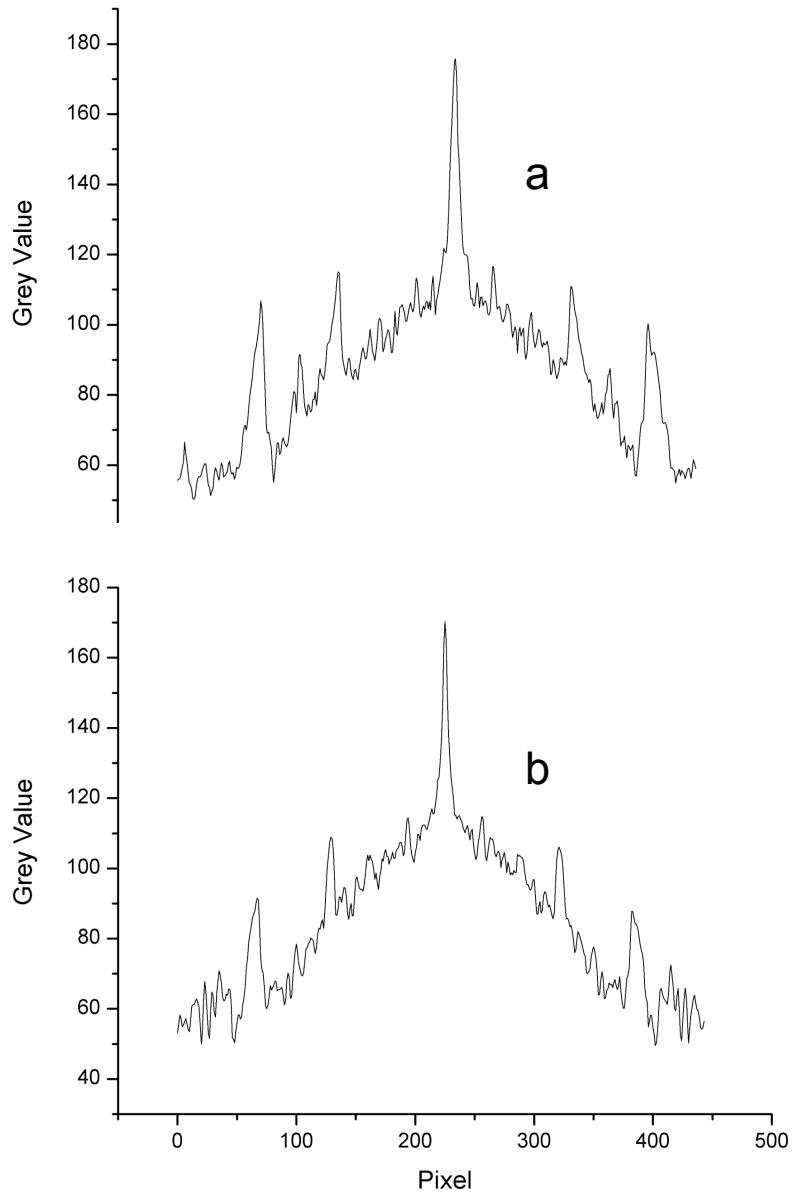
Figure 3.6: Cross-section of the peaks of the Fourier transform for samples a) 2 and b) 4.
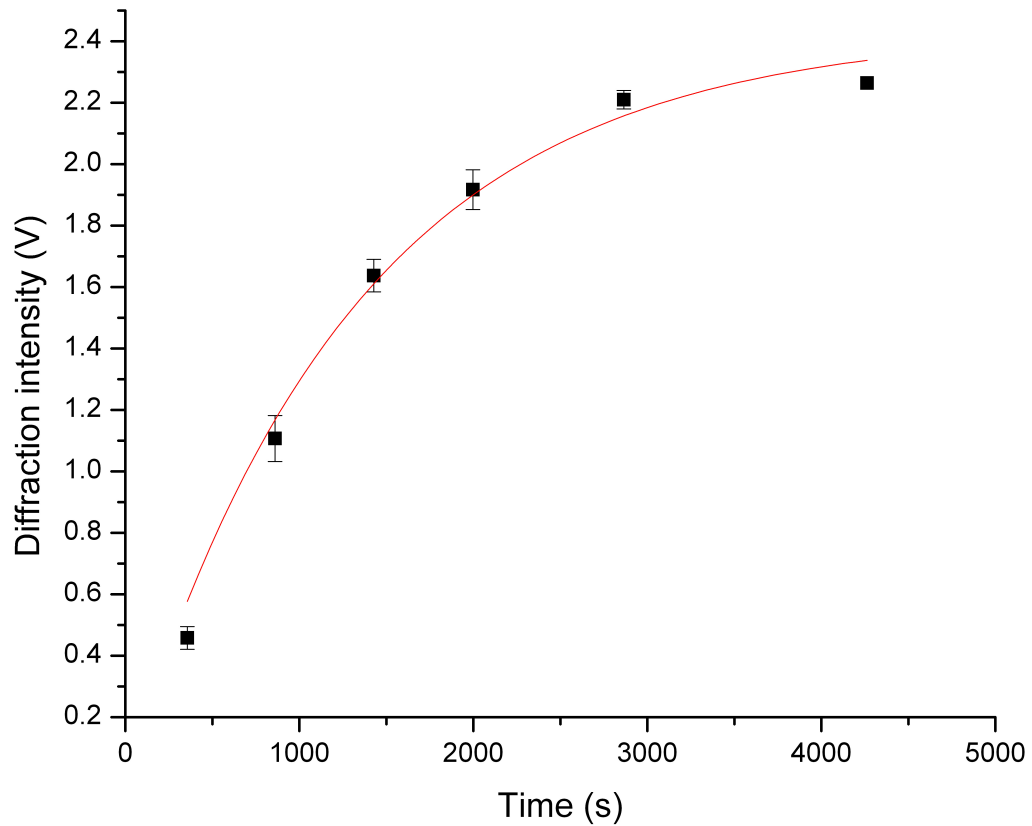
Figure 3.7: Plot showing the measured diffraction intensity as a function of time. The line is a single exponential fit to the data, $y = (2.434(1 - e^{-7.593 \times 10^{-4} x})$
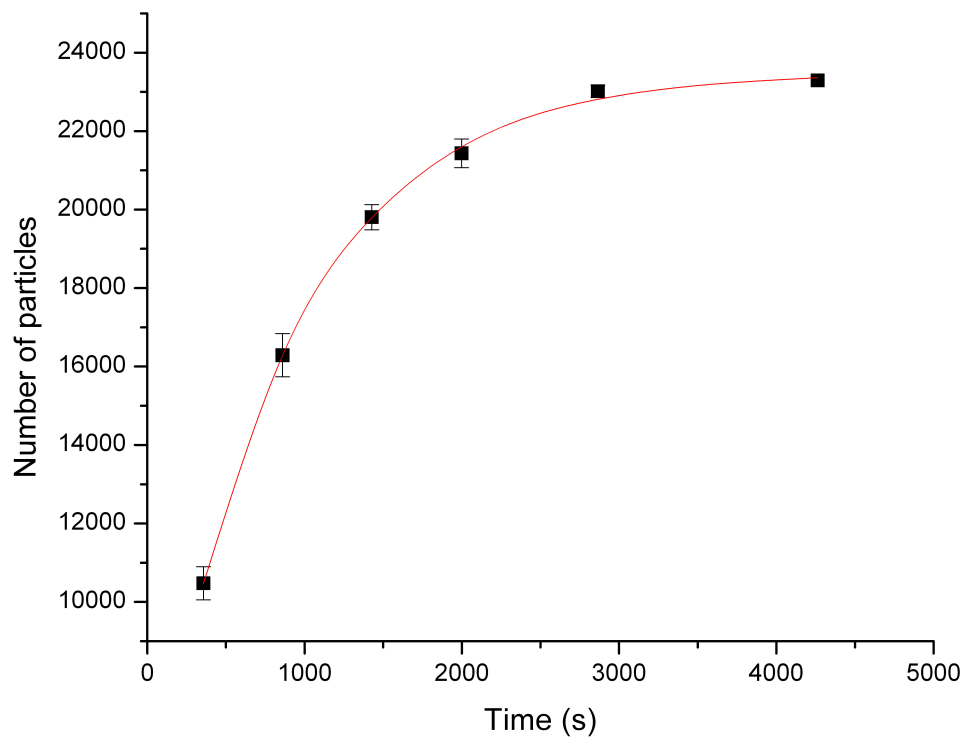
Figure 3.8: Plot of number of particles on the grating surface as a function of incubation time. The number of particles was derived from diffraction intensity using the relation derived from Figure 3.4. The line is a guide to the eye.

CHAPTER 4

CONCLUSIONS AND FUTURE WORK

4.1 Conclusions

In this thesis, two approaches have been taken to gain a better understanding of and to quantify the factors that affect the intensity of the diffraction signal (diffraction efficiency). Initially, a mathematical description of how the diffraction based sensor is expected to operate was developed based on the formalism derived for volume-phase holography. These two approaches investigated the effects of the grating properties, and the effects of analyte loading on signal intensity. The grating properties that were of primary interest are the effects of thickness and refractive index. This was accomplished by developing a series of gratings from polyelectrolyte multilayers. The thickness of the polyelectrolyte gratings was controlled by manipulating the number of layers of polyelectrolyte used and the salt concentration of the polyelectrolyte solutions. Refractive index of these gratings was then manipulated by incorporating gold nanoparticles into the gratings.

The effects of analyte loading and ordering were investigated at the lab of M. Cynthia Goh at the University of Toronto. Using the Axela dotLab^{TM} system, a solution of 2 μm PS beads with carboxyl groups on the surface was flowed over an avidin grating varying the time of exposure of the grating to the beads. The resulting diffraction intensity as a function of time data were interpreted to give kinetic parameters of the system, and to correlate this with the thickness of the sample. Optical microscopy of the sensor surface was then used to elucidate the effect of loading large particles onto the grating surface, and the effects of particle order on the signal.

The formalism that describes volume-phase holography introduces a parameter, diffraction efficiency, which describes the ratio of the intensity of the diffraction spots to the intensity of light initially emitted from the laser. In this relationship, diffraction efficiency has a sine-squared dependence on the thickness of the grating and the variation of refractive index between the grating and the surrounding medium. Using the Taylor expansion, and knowing that we have a limited range of grating thickness and variations in refractive index we developed a simplified relationship where diffraction efficiency exhibits a quadratic dependence on grating thickness and variation in refractive index. Since diffraction efficiency is just a ratio of the diffraction intensity over the intensity of light emitted from the laser, we showed that our observed diffraction intensity should show a quadratic dependence on the grating thickness as well as the variations in refractive index.

A series of diffraction gratings fabricated from polyelectrolyte multilayers were used to determine how well the DBS systems follow mechanism described by VPH theory. Gratings were made using the multilayer microcontact printing technique and were characterized using AFM. The diffraction intensity for these gratings showed a quadratic dependence on the thickness of the gratings as predicted by VPH theory. Polyelectrolyte diffraction gratings were loaded with DMAP stabilized gold nanoparticles to change the refractive index difference between the diffraction gratings and the surrounding media. The diffraction gratings were immersed into the aqueous nanoparticle solutions for approximately 5 minute intervals. AFM images of the diffractions showed that as the diffraction grating is allowed to incubate in the nanoparticle solution for longer periods of time, more nanoparticles adsorb onto the grating surface, increasing the difference in refractive index between the grating and the surrounding media. The diffraction intensity showed a linear dependence on the amount of time the grating was allowed to incubate in the nanoparticle solution.

DBS systems operate by monitoring the change in intensity of a diffraction spot as analyte molecules bind onto the diffraction grating. The major factor that causes the observed change in diffraction intensity is the new optical path length where an analyte molecule is bound to the surface. As large particles of carboxylated PS

are bound onto an avidin grating diffraction intensity increases quadratically. This confirms the expectation large particles act as a thicker grating.

We started to work on a method to determine the degree of order that the particles arranged on the grating surface. This was accomplished by interpreting the Fourier transform of optical images of the PS beads on the grating surface. Our large PS beads should have loaded onto the surface with relatively similar degrees of order as determined by the relationship between diffraction intensity and number of particles of the surface. Within the limits of the detection of our technique, the degree of order of the PS beads on the surface of our grating was the same for all the samples.

We showed, for the first time, the use of a DBS system to obtain the rate and maximum surface coverage of carboxylated PS beads on an avidin surface. The initial rate of this adsorption was shown to be is $16.26 \frac{particles}{s}$. We also determined that the maximum surface concentration of the PS beads on this surface to be 20230 particles mm^{-2}.

4.2   Future Work

There are three areas that need to be addressed to remove any outstanding ambiguities in the understanding of how a DBS operates. The first is to create a variety of diffraction gratings with well defined refractive indices and quantify the relationship between diffraction intensity and the difference in refractive index between the grating and the surrounding media. The second is to use the method developed to quantify the degree to which the particles on the surface reduce the periodicity of the gratings, and gain an understanding of how this effects the observed diffraction intensity. Finally, expanding on the kinetic data to develop a method that will allow mechanistic data to be extracted from the DBS, such as rate constants and activation energies would expand the applicability of the DBS from a purely diagnostic tool.

It has been shown recently that the multilayer thin films can be fabricated using titanium(IV) bis(ammonium lactato)dihidroxide (TALH) and the polyelectrolyte PDAC[32, 33, 34]. The technique for developing these thin films is analogous to the

layer-by-layer (LBL) technique for creating multilayers from two oppositely charged polyelectrolytes. The average refractive index of these films was determined to be 1.68 [34]. In theory this can be combined with traditional LBL polyelectrolyte printing (i.e with two polyelectrolytes) to vary the refractive index of the sample, by changing the concentration of TALH in the samples.

To complete the quantification of particle order on the gratings surface, particles that are significantly smaller than the width of a grating line should be used. Using these particles will allow a greater number of possible configurations of the particles on the surface. Since a large number of these samples will be representative of the large number of possible configurations of the particles on the surface, using the Fourier Transform technique developed here with a series of samples with smaller particles used the dependance of the order of the particles on the observed diffraction intensity can be established.

Finally, information on the order of the reaction and a pseudo rate constant of the adsorption of analyte molecules can be obtained from the dotLab^{TM} system. By performing a series of experiments on the same system (i.e same analyte/grating interaction), varying the concentration of the analyte molecule, one can use the method of initial rates to elucidate the order of the reaction with respect to the analyte molecule. This methodology should work as long as the diffraction intensity curves can be fit to a similar single exponential function as was used in this work so the rate can be determined. Also, the conditions must hold for the method of initial rates to be valid. A pseudo rate constant can also be determined through the same methodology.

References

[1] Y. G. Tsay, C. I. Lin, E. K. Gustafson, R. Appelqvist, P. Magginetti, R. Norton, N. Teng, and D. Charlton. Optical biosensor assay. *Clinical Chemistry*, 37(9):1502–1505, 1991.

[2] J. B. Goh, R. W. Loo, and M. C. Goh. Label-free monitoring of multiple biomolecular binding interactions in real-time with diffraction-based sensing. *Sensors and Actuators B-Chemical*, 106(1):243–248, Apr 2005.

[3] J. B. Goh, P. L. Tam, R. W. Loo, and M. C. Goh. A quantitative diffraction-based sandwich immunoassay. *Analytical Biochemistry*, 313:262–266, 2002.

[4] R. W. Loo, P. L. Tam, J. B. Goh, and M. C. Goh. An enzyme-amplified diffraction-based immunoassay. *Analytical Biochemistry*, 337(2):338–342, Feb 2005.

[5] J. B. Goh, R. W. Loo, R. A. McAloney, and M. C. Goh. Diffraction-based assay for detecting multiple analytes. *Analytical Bioanalytical Chemistry*, 374:54–56, 2002.

[6] P. T. Fiori and M. F. Paige. Detection of enzymatic activity by means of a diffraction based biosensor. *Analytical Bioanalytical Chemistry*, 380:339–342, 2004.

[7] P. M. St. John, R. Davis, N. Cady, J. Czajka, C. A. Batt, and H. G. Craighead. Diffraction-based cell detection using a microcontact printed antibody grating. *Analytical Chemistry*, 70(6):1108–1111, 1998.

[8] R. C. Bailey and J. T. Hupp. Real-time multicolor dna detection with chemoresponsive diffraction gratings and nanoparticle probes. *Journal of the American Chemical Society*, 125(17):13541–13547, October 2003.

[9] X. Dang, K. J. Stevenson, and J. T. Hupp. Monitoring molecular adsorption on high area titanium dioxide via modulated diffraction of visible light. *Langmuir*, 17(11):3109–3112, May 2001.

[10] G. A. Mines, B.-C. Tzeng, K. J. Stevenson, J.-L. Li, and J. T. Hupp. Micropourous supramolecular coordination compounds as chemosensory photonic lattices. *Angewandte Chemie International Edition*, 41(1):154–157, Jan 2002.

[11] F. Nakajima, Y. Hirakawa, T. Kaneta, and T. Imasaka. Diffractive optical chemical sensor based on light absorption. *Analytical Chemistry*, 71(13):2262–2265, 1999.

[12] R. C. Bailey and J. T. Hupp. Micropatterned polymeric gratings as chemoresponsive volatile organic compund sensors: Implications for analute detection and identification via diffraction-based sensor arrays. *Analytical Chemistry*, 75(10):2392–2398, May 2003.

[13] F. G. Kaspar. Diffraction by thick, periodically stratified gratings with complex dielectric constant. *Journal of the Optical Society of America*, 63(1):37–45, 1973.

[14] R. C. Bailey and J. T. Hupp. Large-scale resonance amplification of optical sensing of volatile compounds with chemoresponsive visible-region diffraction gratings. *Journal of the American Chemical Society*, 124(23):6767–6774, May 2002.

[15] S. C. Barden, J. A. Arns, W. S. Colburn, and J. B. Williams. Volume-phase holographic gratings and the efficiency of three simple volume-phase holographic gratings. *Publications of the Astronomical Society of the Pacific*, 112:809–820, 2000.

[16] H. Kogelnik. Coupled wave theory for thick hologram gratings. *The Bell System Technical Journal*, 48(9):2909–2947, Nov 1969.

[17] R. Magnusson and T. K. Gaylord. Analysis of multiwave diffraction of thick gratings. *Journal of the Optical Society of America*, 67(9):1165–1170, 1977.

[18] M. G. Moharam and T. K. Gaylord. Rigorous coupled-wave analysis of planar-grating diffraction. *Journal of the Optical Society of America*, 71(7):811–818, 1981.

[19] A. Bernard, E. Delamarche, H. Schmid, B. Michel, H. R. Bosshard, and H. Biebuyck. Printing patterns of protiens. *Langmuir*, 14(9):2225–2229, 1998.

[20] G. Decher, J. D. Hong, and J. Schmitt. Buildup of ultrathin mulitlayer films by a self-assembly process: Iii. consecutively alternating adsorption of anionic and cationic polyelectrolytes on charged surfaces. *Thin Solid Films*, 1-2(831-835), 1992.

[21] G. Decher, J. Maclennan, U. Sohling, and J. Reibel. Creation and structural comparison of ultrathin film assemblies - transferred freely suspended films and langmuir-blodgett films of liquid crystals. *Thin Solid Films*, 210(1-2):504–507, Apr 1992.

[22] R. A. McAloney, M. Sinyor, V. Dudnik, and M. C. Goh. Atomic force microscopy studies of salt effects on polyelectrolyte multilayer film morphology. *Langmuir*, 17(21):6655–6663, 2001.

[23] F. Davis and S. P. J. Higson. Structured thin films as functional components within biosensors. *Biosensors & Bioelectronics*, 21:1–20, 2005.

[24] B. F. Abu-Sharkh. Structure and mechanism of formation of polyelectrolyte multilayers. *Polymer*, 47:3674–3680, 2006.

[25] J. Park and P. T. Hammond. Multilayer transfer printing for polyelectrolyte multilayer patterning: Direct transfer of layer-by-layer assembled micropatterned thin films. *Advanced Materials*, 16(6):520–525, March 2004.

[26] D. I. Gittins and F. Caruso. Spontaneous phase transfer of nanoparticle metals from organic to aqueous media. *Angewandte Chemie International Edition*, 40(16):3001–3004, 2001.

[27] D. I. Gittins, A. S. Susha, B. Schoeler, and F. Caruso. Dense nanoparticulate thin films via gold nanoparticle self-assembly. *Advanced Materials*, 14(7):508–512, Apr 2002.

[28] IEE- Nanobiotechnology. *Freestanding polyelectrolyte multilayers as functional and constructional elements*, number 4, 2006.

[29] A. Nolte, M. F. Rubner, and R. E. Cohen. Creating effective refractive index gradients within polyelectrolyte multilayer films: Molecularly assembled rugate filters. *Langmuir*, 20(8):3304–3310, 2004.

[30] M. F. Paige, E. J. Bjerneld, and W. E. Moerner. A comparison of through-the-objective total internal reflection microscopy end epiflourescence microscopy for single molecule flourescence imaging. *Single Molecules*, 2(3):191–201, 2001.

[31] http://www.axelabiosensors.com/prods/index.html August 13, 2007. 2006.

[32] J. H. Rousse and G. S. Fergusson. Stepwise formation of ultrathin films of a titanium (hydr)oxide by polyelectrolyte-assisted adsorption. *Advanced Materials*, 14(2):151–154, 2002.

[33] J.-H. Kim, S. Fujita, and S. Shiratori. Design of a thin film for optical applications, consisting of high and low refractive index multilayers, fabricated by a layer-by-layer self-assembly method. *Colloids and Surfaces*, 284:290–294, 2006.

[34] X. Shi, T. Cassagneau, and F. Caruso. Electrostatic interactions between polyelectrolytes and a titania precursor: Thin film and solution studies. *Langmuir*, 18(3):904–910, 2002.

[35] M. Biesalski and J. Ruhe. Preparation and characterization of a polyelectrolyte monolayer covalently attached to a planar solid surface. *Macromolecules*, 32(7):2309–2316, 1999.

[36] A. N. Cartwright and D. V. Nicolau, editors. *Invesigation of the operating mechanism of a diffraction based sensor*, volume 6447, P.O. Box 10 Bellingham, Washington 98227 USA, Jan 2007. SPIE, SPIE.

[37] F. Caruso, H. Lichtenfeld, and H. Mohwald. Investigation of electrostatic inter-actions in polyelectrolyte multilayer films: Binding of anionic fluorescent probes to layers assembled onto colloids. *Macromolecules*, 32(7):2317–2328, 1999.

[38] J. Cho, H. Jang, B. Yeom, H. Kim, R. Kim, S. Kim, K. Char, and F. Caruso. Modulating the pattern quality of micropatterned multilayer films prepared by layer-by-layer self-assembly. *Langmuir*, 22(3):1356–1364, Jan 2006.

[39] P. C. Hidber, W. Helbig, E. Kim, and G. M. Whitesides. Microcontact print-ing of palladium colloids: Micron-scale patterning by electroless deposition on copper. *Langmuir*, 12(5):1327–1380, 1996.

[40] H. Liao, W. Lu, W. Wen, and G. K. L. Wong. Optical characteristics of gold nanoparticle-doped multilayer thin films. *Journal of the Optical Society of America B*, 22(9):1923–1926, Sept 2005.

[41] Y. Lvov, K. Ariga, I. Ichinose, and T. Kunitake. Assembly of multicomponent protein films by means of electrostatic layer-by-layer adsorbtion. *Journal of the American Chemical Society*, 117(22):6117–6123, 1995.

[42] F. Morhard, J. Pipper, R. Dahint, and M. Grunze. Immobilizationo of anti-bodies in micropatterns for cell detection by optical diffraction. *Sensors and Actuators B-Chemical*, 70:232–242, Nov 2000.

[43] K. A. Nelson, R. Casalegno, R. J. D. Miller, and M. D. Fayer. Laser-induced excited state annd ultrasonic wave gratings: Amplitude and phase grating con-tributions to diffraction. *Journal of Chemical Physics*, 77(3):1144–1152, 1982.

[44] L. B. Scaffardi and J. O. Tocho. Size dependence of refractive index of gold nanoparticles. *Nanotechnology*, 17:1309–1315, 2006.

[45] K. S. Schanze, T. S. Bergstedt, B. T. Hauser, and C. S. P. Cavalaheiro. Photolithographically-patterned electroactive films and electrochemically mod-ulated diffraction gratings. *Langmuir*, 16(2):795–810, 2000.

[46] A. N. Shipway, E. Katz, and I. Willner. Nanoparticle arrays on surfaces for electronic optical and sensor applications. *ChemPhysChem*, 1(1):18–52, 2000.

Appendix A

LabView Routine

The LabView software package was used to develop a routine to output the diffraction intensity observed by our photodetector by Luanne Sawatzsky. The program outputs two charts, one is of raw data over the averaging time period, the other plots each time averaged signal as a function of time.

averaged_analysis_6.vi
C:\Users\J\averaged_analysis_6.vi
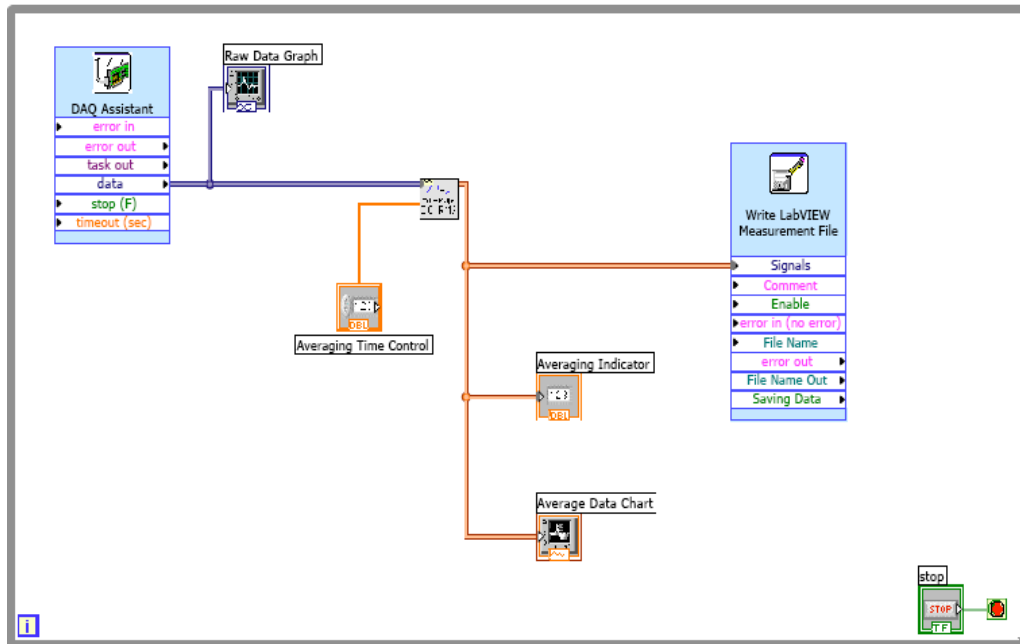Last modified on 14/05/2004 at 4:17 PM
Printed on 25/10/2007 at 1:40 PM

Figure A.1: Screen shot of LabView routine used to measure diffraction intensity